© 2021. Published by The Company of Biologists Ltd | Journal of Cell Science (2021) 134, jcs252189. doi:10.1242/jcs.252189

RESEARCH ARTICLE

The voltage-gated sodium channel β2 subunit associates with lipid rafts by S-palmitoylation

Eric Cortada[1,2], Robert Serradesanferm[1,2,*], Ramon Brugada[1,2,3,4] and Marcel Verges[1,2,3,‡]

ABSTRACT

The voltage-gated sodium channel is critical for cardiomyocyte function. It consists of a protein complex comprising a pore-forming α subunit and associated β subunits. In polarized Madin–Darby canine kidney cells, we show evidence by acyl-biotin exchange that β2 is S-acylated at Cys-182. Interestingly, we found that palmitoylation increases β2 association with detergent-resistant membranes. β2 localizes exclusively to the apical surface. However, depletion of plasma membrane cholesterol, or blocking intracellular cholesterol transport, caused mislocalization of β2, as well as of the non-palmitoylable C182S mutant, to the basolateral domain. Apical β2 did not undergo endocytosis and displayed limited diffusion within the plane of the membrane; such behavior suggests that, at least in part, it is cytoskeleton anchored. Upon acute cholesterol depletion, its mobility was greatly reduced, and a slight reduction was also measured as a result of lack of palmitoylation, supporting β2 association with cholesterol-rich lipid rafts. Indeed, lipid raft labeling confirmed a partial overlap with apical β2. Although β2 palmitoylation was not required to promote surface localization of the α subunit, our data suggest that it is likely implicated in lipid raft association and the polarized localization of β2.

KEY WORDS: Protein sorting, Palmitoylation, Voltage-gated sodium channel, *SCN2B*, $Na_V1.5$, Cardiac arrhythmia

INTRODUCTION

Cardiac arrhythmia may lead to sudden death. Many genetic disorders can bring about arrhythmias often not associated with structural heart alterations. These are considered inherited channelopathies caused by mutations in ion channels that give rise to alterations in the generation or propagation of the action potential. Alterations in functioning of voltage-gated sodium (Na_V) channels can thus lead to cardiac channelopathies (Amin et al., 2010). Brugada syndrome is a clear example of an arrhythmia mostly associated with the loss-of-function of $Na_V1.5$, a large multi-pass transmembrane protein forming the pore of the major cardiac Na_V channel (Napolitano and Priori, 2006). Loss-of-function is frequently caused by defective $Na_V1.5$ trafficking and localization to the cell surface (Rook et al., 2012).

[1]Cardiovascular Genetics Group, Girona Biomedical Research Institute (IDIBGI), 17190 Salt, Prov. Girona, Spain. [2]Biomedical Research Networking Center on Cardiovascular Diseases (CIBERCV), 17190 Salt, Prov. Girona, Spain. [3]Medical Sciences Department, University of Girona Medical School, 17071 Girona, Spain. [4]Cardiology Department, Hospital Josep Trueta – University of Girona Medical School, 17007 Girona, Spain.
*Present address: Hipra Scientific S.L.U., 17170 Amer, Prov. Girona, Spain

‡Author for correspondence (mverges@gencardio.com; marcel.verges@udg.edu)

E.C., 0000-0002-3217-4465; R.S., 0000-0002-7635-0467; R.B., 0000-0001-6607-3032; M.V., 0000-0002-2606-223X

Handling Editor: John Heath
Received 24 July 2020; Accepted 8 February 2021

The Na_V channel α subunit is part of a macromolecular protein complex located in different microdomains of the cardiomyocyte sarcolemma. It is now clear that $Na_V1.5$ interacts, directly or indirectly, with proteins involved in diverse cellular roles, such as cytoskeleton anchoring, signal transduction and cell-cell adhesion (Rivaud et al., 2020), whose alteration can cause arrhythmia (Kyle and Makielski, 2014). In addition, associated β subunits regulate the localization and function of the Na_V channel (O'Malley and Isom, 2015).

The β subunit family consists of four genes, *SCN1B*, *SCN2B*, *SCN3B* and *SCN4B*. Respectively, these encode β1–4, of which β1 has two alternative splice variants, β1A and β1B (Brackenbury and Isom, 2011). With the exception of β1B, all share a similar membrane topology, which includes an N-terminal extracellular immunoglobulin-like loop, with a cell adhesion role, a single transmembrane domain (TMD) and a short C-terminal intracellular domain (ICD) (O'Malley and Isom, 2015). Early work showed the implication of β2 in controlling Na_V channel localization (Schmidt and Catterall, 1986; Zimmer et al., 2002) which, like β4, interacts with α by a disulfide bond (Chen et al., 2012). We previously described a Brugada syndrome-associated mutation in *SCN2B* causing a 40% decrease in sodium current density due to reduced surface levels of $Na_V1.5$ (Dulsat et al., 2017; Riuro et al., 2013). Consistent with those data, *Scn2b* deletion in mice causes comparable effects in ventricular myocytes (Bao et al., 2016) and in primary cultures of hippocampal neurons (Chen et al., 2002).

Using a polarized cellular model – Madin–Darby canine kidney (MDCK) cells – we have shown that exogenously expressed β2 is transported in a polarized fashion, namely, to the apical plasma membrane (PM) (Dulsat et al., 2017). However, it is not known how β2 localizes preferentially to this surface domain. Understanding how apical targeting signals are recognized in proteins has been the focus of intense study. Detection can certainly be mediated by association of the TMD of the protein with glycosphingolipid/cholesterol-rich membrane domains, i.e. lipid rafts. It can also occur via *N*- or *O*-glycosylation of the luminal domain, and subsequent interaction with carbohydrate-binding lectins. Members of the Ras superfamily of small Rab GTPases, microtubule motors and the actin cytoskeleton have also been implicated (Stoops and Caplan, 2014; Weisz and Rodriguez-Boulan, 2009). In this regard, we have demonstrated that *N*-glycosylation is required for the efficient trafficking and localization of β2 to the PM, as lack of glycosylation causes its retention in the endoplasmic reticulum (ER) (Cortada et al., 2019a).

Ion channels, including $Na_V1.5$, are grouped into functional microdomains in subregions of the sarcolemma (Gillet et al., 2014). An interesting hypothesis envisaged is that this association can be aided through interaction with lipid rafts, which have been shown to include ion channel-regulatory proteins (Balse et al., 2012), and correspond to the 'liquid-ordered (Lo) phase' of the membrane (Kusumi et al., 2020). Palmitoylation, which is the most common form of S-acylation, plays a key role in targeting to lipid rafts

Journal of Cell Science (2021) 134, jcs252189. doi:10.1242/jcs.252189

(Aicart-Ramos et al., 2011), and this in turn appears to be required for apical delivery (Simons and Sampaio, 2011). Indeed, it is long known that depletion of cellular cholesterol reduces apical protein transport, causing missorting, but leaving basolateral transport unaffected (Keller and Simons, 1998). In this study, we have investigated the role of palmitoylation in subcellular localization and dynamics within the membrane of β2. Using heterologous expression in MDCK cells, we show that β2 is palmitoylated at its conserved Cys-182. We found that palmitoylation increases β2 affinity for lipid raft domains and appears to be implicated in its polarized localization.

RESULTS

Evidence of β2 palmitoylation

We previously found that *N*-glycosylation is required for the efficient trafficking and localization of β2 to the PM (Cortada et al., 2019a). In polarized MDCK cells, exogenously expressed β2 localizes to the apical domain (Dulsat et al., 2017). β2 has a single conserved Cys residue in its ICD that may be palmitoylated, i.e. Cys-182 (Chopra et al., 2007). Palmitoylation can increase protein affinity for glycosphingolipid/cholesterol-rich raft domains (Aicart-Ramos et al., 2011), and detection of apical signals may be mediated by lipid raft association (Stoops and Caplan, 2014; Weisz and Rodriguez-Boulan, 2009). It is thus plausible to consider that this post-translational modification may influence the preferential apical localization of β2. Therefore, in this study we hypothesized that β2 can be palmitoylated. We aimed to detect β2 palmitoylation by an acyl-biotin exchange (ABE) assay, performed essentially as described for nonradioactive samples (Drisdel and Green, 2004). To facilitate β2 reaching its steady state localization, we used stable MDCK cell lines. YFP-tagged β2 was first immunoprecipitated in the presence of N-ethylmaleimide (NEM). A band at ∼80 KDa, corresponding to the molecular weight of fully glycosylated β2-YFP (Cortada et al., 2019a), was effectively detected by anti-biotin blot in immunoprecipitates after BMCC-Biotin labeling under hydroxylamine (HAM) treatment; HAM selectively reduces thiols attached to palmitate. Evidence of specificity was confirmed by the absence of biotinylated β2 in immunoprecipitates using an irrelevant antibody – specifically, against vacuolar protein sorting (VPS) 26A, a major endosomal protein (Mellado et al., 2014) – and in native MDCK cells (Fig. 1A).

This experiment shows the presence of a reactive Cys that can be hydrolyzed by HAM, which enables it to be biotinylated. We therefore mutated Cys-182 to Ser (C182S), which is expected to render a non-palmitoylable protein. By ABE, β2 biotinylation was greatly reduced in immunoprecipitates from β2 C182S-expressing cells treated with HAM compared with those from cells with β2 wild type (Fig. 1B-E). Evidence that NEM effectively blocked free Cys residues in immunoprecipitations was seen by the presence, when NEM was omitted, of several non-specific bands, resulting from free thiol groups, not susceptible to cleavage by HAM, and later biotinylated, which were absent when NEM was included (empty arrowheads in Fig. S1). Moreover, the reaction was inhibited under increasing concentrations of the palmitate analog 2-bromopalmitate (also known as 2-bromohexadecanoic acid, 2-BP), which acts as a palmitoylation inhibitor in live cells (Fig. 1D,E). Although the assay performed does not involve incorporation of radioactive palmitate, our data provide biochemical evidence that β2 is, with a high probability, palmitoylated at Cys-182 in cells.

β2 association to detergent-resistant membranes relies on palmitoylation

Next, we addressed whether β2 palmitoylation influences its subcellular localization, including possibly its apical delivery (Simons and Sampaio, 2011). We took a biochemical approach to test the potential association of β2 to PM subdomains that may be representative of lipid rafts, defined as the Lo phase of the membrane (Kusumi et al., 2020). To this end, we isolated detergent-resistant membranes (DRMs) from cell extracts solubilized with a non-ionic detergent at 4°C (Reverter et al., 2011). In agreement with published data (Wong et al., 2005), β2 wild type was partially recovered in the upper 2 to 3 fractions of the sucrose gradient, in which both raft-associated flotillin-1 and caveolin-1 concentrate (Fig. 2A). Blotted protein bands were quantified and their normalized abundance was plotted (Fig. 2B). An estimate suggests that the relative portion of β2 within DRM is ∼12% of total β2 in all fractions collected. On the contrary, β2 C182S was barely detected in these DRM fractions, similar to non-raft Na/K-ATPase, both found exclusively in the lower two thirds of the gradient, and therefore can be considered completely Triton X-100 soluble (Fig. 2A,C). Indeed, quantification showed that only ∼4% of β2 C182S falls within DRM fractions. Yet, it must be kept in mind that these values may be somewhat overestimated due to the comparatively much higher band intensities of β2 in detergent-soluble fractions. Thus, these data show that palmitoylation of Cys-182 increases β2 affinity for DRM and, therefore, it may be implicated in its association to the membrane Lo phase.

The polarized localization of β2 is dependent on cholesterol

We next examined whether cholesterol-rich raft domains at the PM are indeed implicated in regulating β2 localization to the cell surface in polarized cells. To this end, we analyzed β2 distribution by surface biotinylation and confocal immunofluorescence microscopy upon cholesterol depletion. Indeed, in cells treated with methyl-β-cyclodextrin (MβCD), a cholesterol-depleting drug (Zidovetzki and Levitan, 2007), β2 lost its exclusive apical localization. Thus, it was comparably detected at the basolateral surface, indicating mislocalization. Evidence that the effect is specific on β2 was seen by proper localization of apically delivered gp114 and basolateral Na/K-ATPase under the same conditions (Fig. 3A).

MβCD sequesters cholesterol from the cell surface, which may gradually reduce cholesterol from intracellular membranes. Cells may try to compensate it by activating cholesterol synthesis. In addition to MβCD, we thus included lovastatin, as an inhibitor of mevalonate synthesis, which is a key reaction in the cholesterol synthesis pathway (Alberts, 1988). In fact, a conspicuous effect was obtained when we analyzed, by immunofluorescence, mislocalization of β2 due to cholesterol depletion in cells acutely treated with MβCD after overnight incubation with 4 µM lovastatin. Thus, while β2 was observed exclusively at the apical surface in untreated cells (Fig. 3B), it redistributed partially to the basal region upon treatment (Fig. 3C). Cell polarity remained unaffected, as seen by the expected location of gp114 and the tight junction marker Zonula Occludens-1 (ZO-1, also known as TJP1). Quantification of fluorescence along apical-to-basal *z*-stacks confirmed that the β2 curve peak, although still coinciding with that of apical gp114 in treated cells, expanded into more nuclear (basal) sections. Thus, the relative fluorescence intensity in the basolateral region, expressed as corrected total cell fluorescence (CTCF), changed from 20-30% of the maximum fluorescence (recorded at the most apical section) to 50-60% (Fig. 3D,E). A comparable effect in the mislocalization of β2 to the basolateral domain was seen after an extended treatment with U18666A, which blocks intracellular cholesterol transport (Cenedella, 2009), along with lovastatin. Similarly, polarity markers, such as Na/K-ATPase and ZO-1, remained unaffected (Fig. S2A,B,E,F).

Thus, the polarized localization of β2 was lost by acute or long-term cholesterol depletion, in either case, causing mislocalization to

Journal of Cell Science (2021) 134, jcs252189. doi:10.1242/jcs.252189

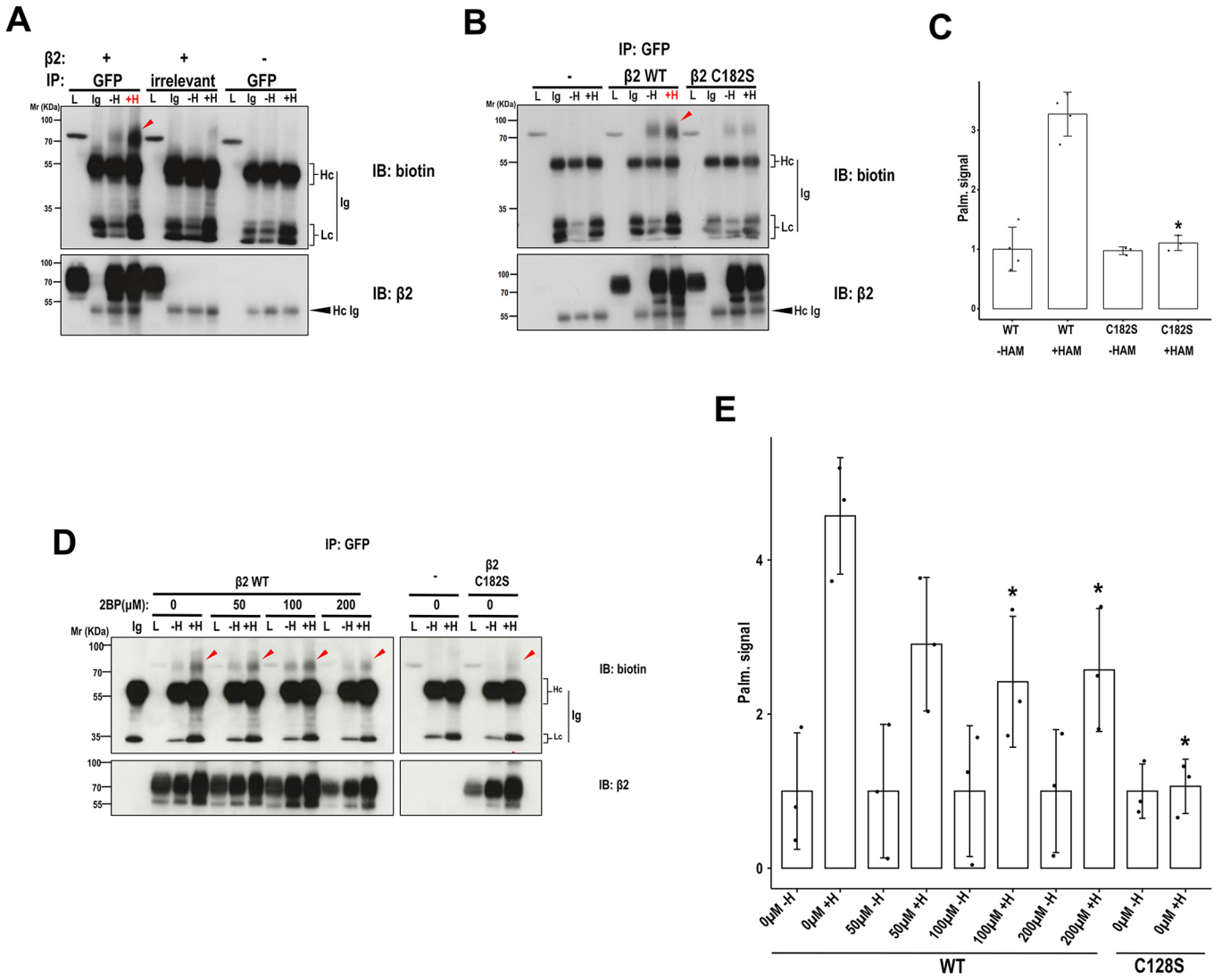

Fig. 1. Palmitoylation of β2 at Cys-182. (A-C) Representative western blots (IB) from an ABE assay (A,B) and band quantification (C) show that β2 wild type (WT, red arrowhead), but not C182S, is likely palmitoylated. (D,E) In the presence of increasing concentrations of 2-BP, the reaction was gradually inhibited (red arrowheads point to the position of biotinylated β2). Cells analyzed were parental (–) or stably expressing β2-YFP, wild type (+) or C182S. HAM treatment of immunoprecipitates (IP) is indicated by +H (with) or –H (without). Ig indicates an equivalent amount of antibody alone processed in parallel. L, lysate; Hc and Lc indicate heavy and light immunoglobulin (Ig) chains, respectively. In anti-biotin blots, note the presence of a non-specific band in lysates migrating as, but unrelated to, β2-YFP. (C,E) Data are expressed as normalized palmitoylation (Palm.) signal. Data are mean±s.d. Differences were highlighted by an unpaired two-tailed Student's *t*-test (C, **P*=0.0013, compared with wild type +HAM) and by one-way ANOVA with Dunnett's post-hoc test (E, wild type +HAM, 0 μM versus 100 μM, **P*=0.0183; versus 200 μM, **P*=0.0268; and versus C182S, **P*=0.0007).

the basolateral membrane. Intriguingly, non-palmitoylable β2 C182S also displayed apical polarity (Fig. S2C, Fig. S3B, Fig. S4A,C) and behaved similarly to the wild type upon cholesterol depletion (Fig. S2C,D,G,H, Fig. S3B, Fig. S4B,D). This indistinguishable behavior suggests that Cys-182, although not required for the steady state apical localization of β2, may still be important for partitioning apically localized β2 to Lo surface domains.

Lack of endocytosis and limited membrane diffusion of β2

These results so far suggest that β2 dynamics within the membrane may be influenced by the cholesterol content, yet the potential contribution of its Cys residue susceptible of palmitoylation still remains unknown. Therefore, we looked at potential β2 internalization. To this end, we biotinylated the apical membrane domain and examined β2 endocytosis upon glutathione cleavage of surface-exposed biotinylated proteins, which leaves intracellular biotin moieties protected. The label from biotinylated β2 was effectively gone after glutathione cleavage, performed at time zero. However, even after 60 min at 37°C, β2 was not detected in pulldowns, similar to gp114, known to display very little endocytosis in MDCK cells (Le Bivic et al., 1993), and cytoplasmic VPS26A (Mellado et al., 2014), not accessible to the biotin reagent (Fig. 4A). As a positive control, we performed the assay in cells transiently expressing β-secretase (BACE1), which localizes to the apical surface and undergoes endocytosis. As expected, its endocytosis was recorded at 15 min, remaining nearly undetected at a later time point, when biotinylated BACE1 has been already recycled, degraded or transported by transcytosis to the basolateral surface (Cuartero et al., 2012), and its biotin moiety has therefore been cleaved by glutathione (Fig. 4B).

As cholesterol depletion caused β2 mislocalization to the basolateral surface (see Fig. 3), we reasoned that the movement of β2 in the plane of the membrane monitored by fluorescence

Journal of Cell Science (2021) 134, jcs252189. doi:10.1242/jcs.252189

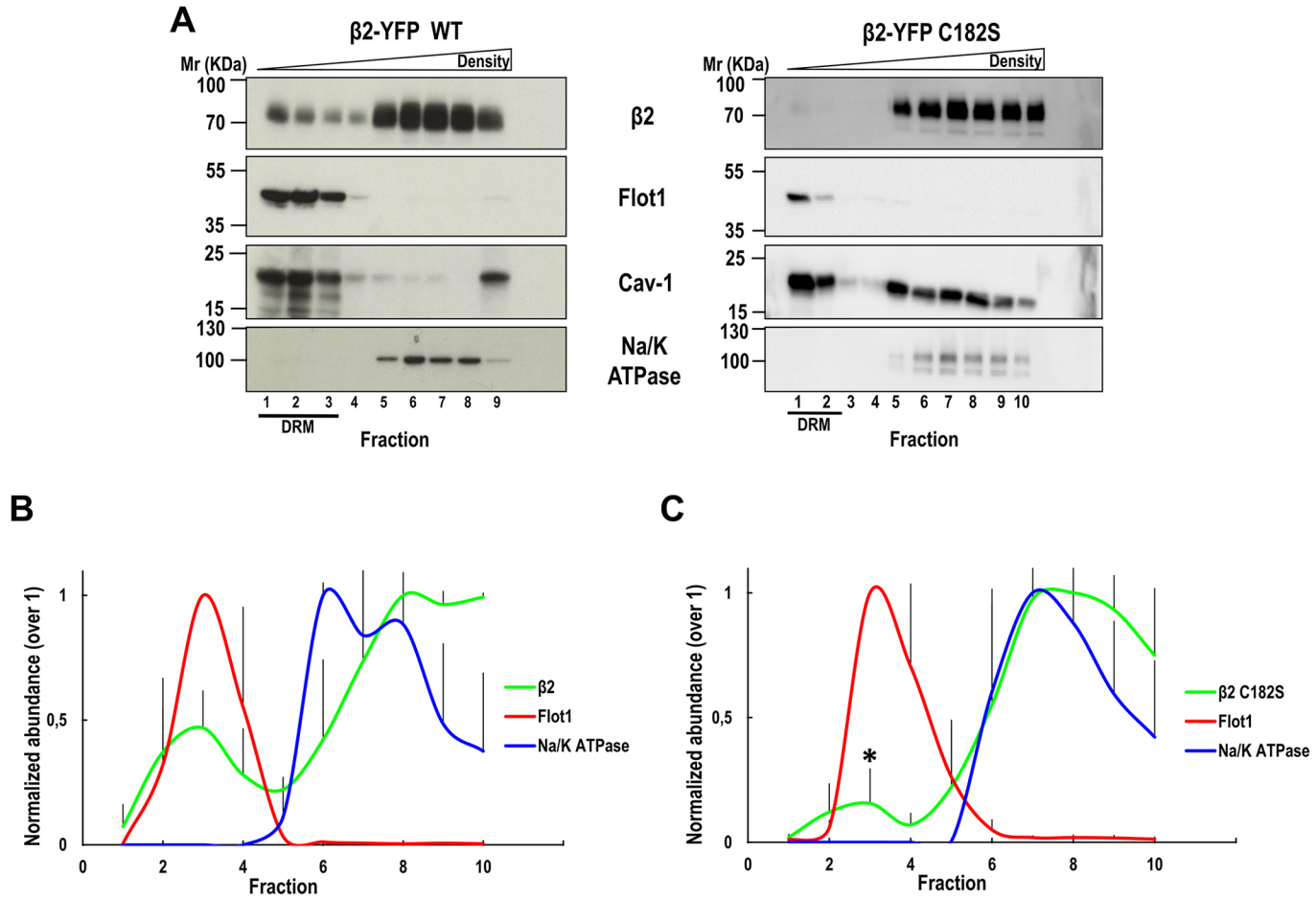

Fig. 2. Palmitoylation of β2 promotes its partition into DRM fractions. (A-C) Representative western blots of isolated fractions (A) and band quantifications (B, C) show a portion of β2 wild type (WT), but not C182S, floating in DRM fractions enriched in flotillin-1 (Flot1), as well as caveolin-1 (Cav-1). Blots for Na/K-ATPase indicate the distribution of this non-raft protein in the lower two-thirds of the gradient. Data are expressed as normalized abundance. An unpaired two-tailed Student's *t*-test showed significant differences in fraction 3 (**P*=0.046). Quantification of the relative β2 signal within the DRM fractions over all fractions collected shows 11.6±3.4% for the wild type compared with 4.2±3.5% by β2 C182S.

recovery after photobleaching (FRAP) in live cells could be affected upon this treatment. As we have seen previously (Cortada et al., 2019a), fluorescence of YFP-tagged β2 generally shows only a partial recovery upon bleaching. This results in a gradually smaller mobile fraction (MF) when increasing the bleached area (Fig. 5A), as often expected (Sprague and McNally, 2005). We therefore performed the analyses using a nominal radius (r_n) of 2 µm, which is the minimum feasible r_n in our set up. Acute cholesterol depletion, with increasing doses of MβCD, dramatically decreased the MF of β2, as measured at the cell end between two adjacent cells (Fig. 5B). However, neither the half-time of recovery ($\tau_{1/2}$) nor the diffusion coefficient (*D*) were affected (Table 1), indicating that the portion of molecules that can undergo diffusion diminished, whereas the rate of diffusion, or speed at which molecules move, did not change.

To obtain insights into the contribution of palmitoylation in the membrane dynamics of β2, we next addressed potential differences between β2 wild type and C182S. Interestingly, the MF of β2 C182S at the cell surface was slightly, yet significantly, decreased compared with the wild type (Fig. 5C). Likewise, $\tau_{1/2}$ displayed a tendency to increase in the mutant, indicative of overall reduced mobility (Table 1). This suggests that a small portion of β2 wild type, i.e. that expected to be available for palmitoylation, may occupy raft domains and display a somewhat increased mobility than when not in these domains, as would be the case of β2 C182S.

The usually slow β2 dynamics also suggests that it may be additionally limited by anchoring to the underlying membrane cytoskeleton. We therefore tested the mobility of β2 lacking its ICD, that is, truncated at residue 181 (181X). Although a small portion of β2 181X reached the apical surface (Fig. S5A), it mostly remained in the ER, as it was completely cleaved by endoglycosidase H (Endo H), to which immature, but not complex, *N*-glycans on ER proteins are sensitive; such was the case of this β2 mutant (Fig. S5B). Strikingly, β2 181X displayed complete fluorescence recovery (Fig. 5D) and moved twice as fast as the wild type (Table 1). Given the dynamic interactions existing between lipid rafts and cytoskeleton elements (Head et al., 2014), this experiment also substantiates evidence that a fraction of β2 associates with Lo membrane domains.

A fraction of β2 colocalizes with lipid rafts

To support our finding that β2 is partially present in Lo membrane domains, we labeled polarized live cells with cholera toxin (CTX), the B subunit (CTB) of which binds to the lipid raft-associated ganglioside GM1 (Janich and Corbeil, 2007), detecting it by subsequent incubation with an anti-CTB antibody. CTX labeling was seen most predominantly apically, with some lateral staining as well (Fig. 6B); the absence of labeling without CTX confirmed specificity of the antibody (Fig. 6A). Interestingly, β2 overlapped

Journal of Cell Science (2021) 134, jcs252189. doi:10.1242/jcs.252189

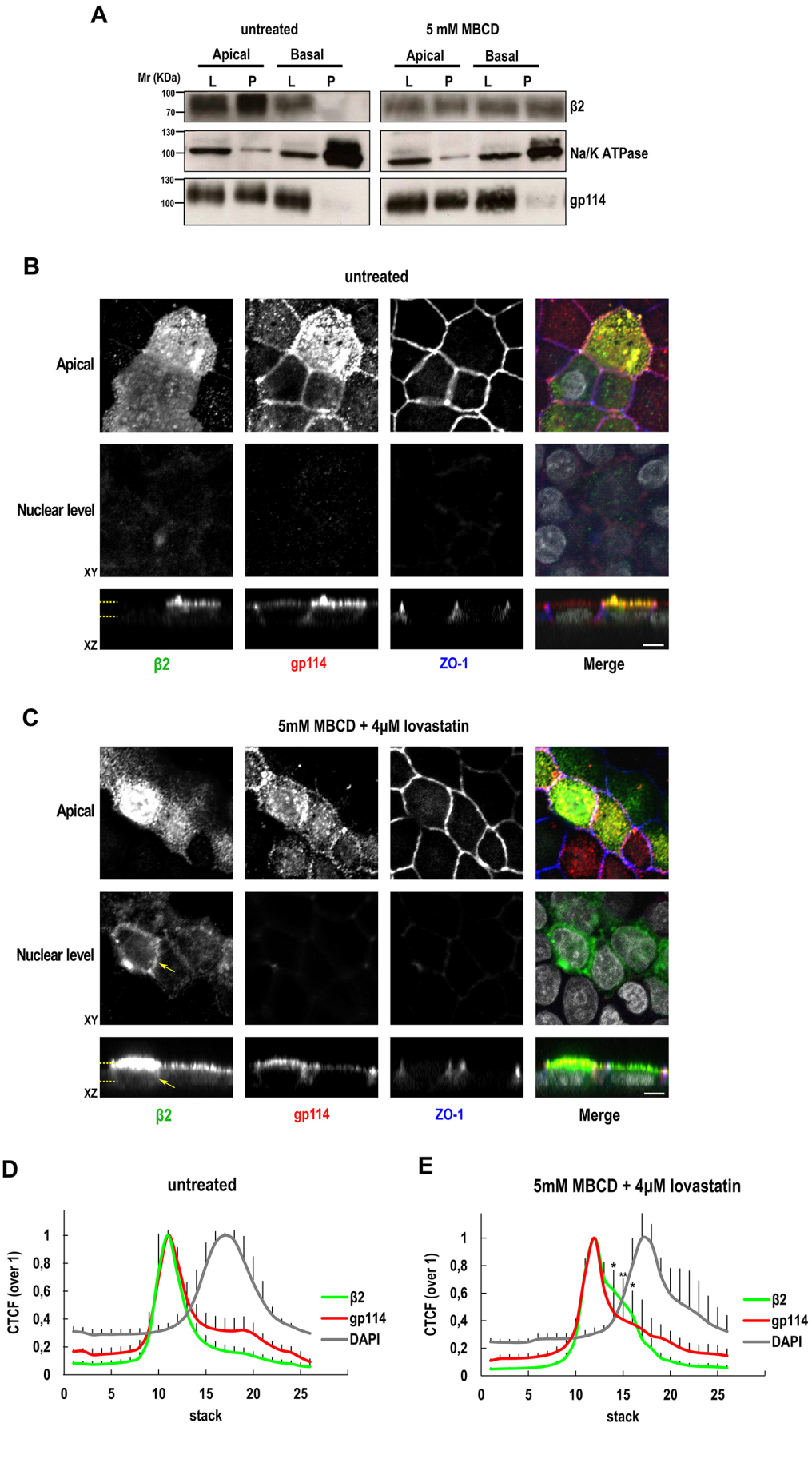

Fig. 3. β2 is mislocalized to the basolateral surface due to cholesterol depletion. (A) Representative western blots of polarized cells transiently expressing β2-CFP wild type show redistribution of β2 to the basolateral surface in the presence of MβCD, whereas the polarity markers gp114 and Na/K-ATPase remain at their apical and basolateral (Basal) domains, respectively, confirming proper cell polarity. P indicates pulldown, whereas L indicates lysate. (B,C) Representative confocal XY sections and corresponding *z*-axis reconstructions (XZ) show that apically localized β2 (green) is also present at the basolateral membrane upon the treatment (yellow arrows in C), whereas gp114 (red) and ZO-1 (blue) remain unaffected. The two parallel yellow dashed lines in XZ mark the sections shown by XY, either apical or nuclear. In merged images, the nuclear staining by DAPI is in grey. (D,E) Line charts displaying the CTCF show the β2 curve peak coinciding with that of apical gp114 (D). The β2 curve extends into more basal sections in treated cells, in part overlapping with DAPI (E), included as reference for the nuclear level. An unpaired two-tailed Student's *t*-test showed significant differences in stacks 14-16 (**P*<0.05, ***P*<0.01). Scale bars: 5 µm.

Journal of Cell Science (2021) 134, jcs252189. doi:10.1242/jcs.252189

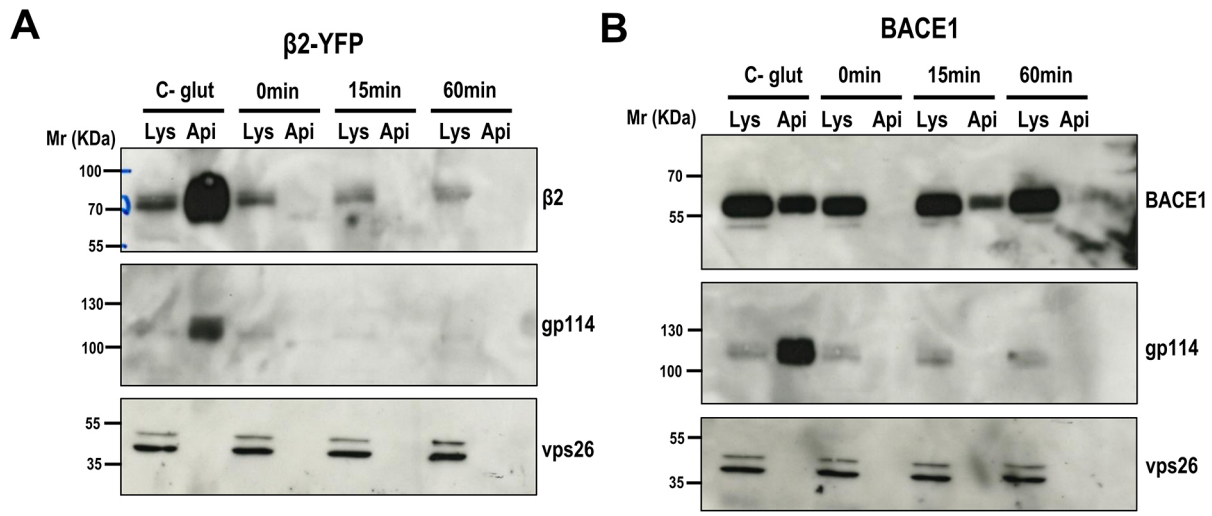

Fig. 4. β2 does not undergo endocytosis. (A,B) Representative western blots of polarized cells transiently expressing β2-YFP wild type (A) or BACE1 (B) show that BACE1 is recovered in pulldowns after 15 min, denoting apical endocytosis, but not β2, at any time point analyzed. 'Api' indicates each pulldown of apically labeled cells, whereas Lys indicates lysate. As a control, note the total absence of biotinylated protein in pulldowns of cells treated with glutathione (glut) immediately after labeling (0 min). In addition, apical gp114 does not get endocytosed and VPS26A (vsp26) is a cytoplasmic protein not accessible to the biotin reagent.

considerably with CTX (Fig. 6C). This was verified by the calculation of their CTCF along *z*-stacks, which showed maximum fluorescence peaks overlapping at apical sections (Fig. 6E). Manders' coefficient, defined here as the fraction of β2 present in CTX^+ compartments (Dulsat et al., 2017), indicated an ∼40% overlap at the apical region.

As with β2 wild type, partial overlap with CTX-labeled raft domains was also seen for β2 C182S (Fig. 6D,F). To ensure that forced crosslinking of the CTX-labeled lipid rafts with the anti-CTB antibody was not causing an apparent overlap, we tested whether colocalization still takes place in fixed cells subsequently labeled with CTX. Here too, both β2 wild type and C182S partially overlapped with CTX-labeled raft domains at the apical surface (Fig. S6). Yet, this similar behavior may be mainly due to limitations of resolution by confocal microscopy, which cannot resolve raft domains.

Palmitoylation of β2 is not required to promote surface localization of $Na_V1.5$

Associated β subunits regulate the localization and function of the Na_V channel (O'Malley and Isom, 2015), and β2 in particular promotes surface localization of $Na_V1.5$ (Cortada et al., 2019b). As $Na_V1.5$ and other ion channels are found in functional membrane microdomains, the organization of which may depend on interactions within lipid rafts (Balse et al., 2012), we were curious about the functional consequences of β2 palmitoylation on $Na_V1.5$. Therefore, we tested whether non-palmitoylated β2 was defective in promoting its surface localization. As expected (Dulsat et al., 2017), a fraction of $Na_V1.5$ colocalized with β2 and the apical marker gp114 (Fig. 7A), which was supported when representing the CTCF along *z*-stacks (Fig. 7C). In the presence of β2 C182S, although $Na_V1.5$ distribution appeared more widespread, with a certain tendency toward the nuclear level, differences with β2 wild type were not significant (Fig. 7B,D). Cell surface biotinylation confirmed the lack of an obvious defect in the presence of β2 C182S, as $Na_V1.5$ reached the cell surface to a similar extent as with β2 wild type (Fig. 7E). Therefore, palmitoylation of β2 does not appear to be required to promote surface localization of $Na_V1.5$; nevertheless, it may still have important implications in regulating β2 association with lipid raft domains and in its polarized localization to the cell surface.

Altogether, these data show that β2 can associate with Lo membrane domains, which can be considered as lipid rafts. Our results provide evidence that palmitoylation increases β2 affinity for these domains. As a fraction of β2, i.e. the potentially palmitoylated β2, partitions into DRM, our data suggest that palmitoylation may contribute in this way to establish its apical localization, and thus its polarized distribution at the cell surface.

DISCUSSION

In this study, we analyzed a potential mechanism regulating trafficking of the Na_V channel β2 subunit that may be the key determinant in ensuring its correct subcellular localization. We provide evidence that β2 is palmitoylated at Cys-182 in cells, and that palmitoylation appears to increase its affinity for DRM. We found that the polarized localization of β2 is dependent on PM cholesterol. Lack of measurable endocytosis, and its modest diffusion within the plane of the membrane, which was further reduced in the non-palmitoylated mutant and especially upon acute cholesterol depletion, give support to the idea that β2 palmitoylation promotes its association with glycosphingolipid/cholesterol-rich raft domains, defined as the Lo phase of the membrane (Kusumi et al., 2020).

Channel-associated β subunits contribute to the proper functioning of their corresponding pore-forming α subunit. In this context, a reported role of β2 in the heart is its involvement in ensuring the surface localization of $Na_V1.5$ (O'Malley and Isom, 2015). However, little is known about how the localization of β subunits themselves is regulated (Cortada et al., 2019b; Salvage et al., 2020). Regarding β2, we recently found that *N*-linked glycosylation is required for its efficient trafficking and PM localization; moreover, lack of glycosylation made β2 defective in promoting surface localization of $Na_V1.5$ (Cortada et al., 2019a). Here, by ABE, we found that β2 is, with high probability, S-acylated at its conserved Cys-182 (Chopra et al., 2007). The most common form of S-acylation is palmitoylation, and this post-translational modification has been implicated in protein targeting to lipid rafts (Aicart-Ramos et al., 2011).

In polarized MDCK cells, in which we carried out our study, β2 localizes strictly to the apical surface (Dulsat et al., 2017). Understanding the mechanisms governing polarized trafficking is of great importance, as alterations in polarity turn into serious

Journal of Cell Science (2021) 134, jcs252189. doi:10.1242/jcs.252189

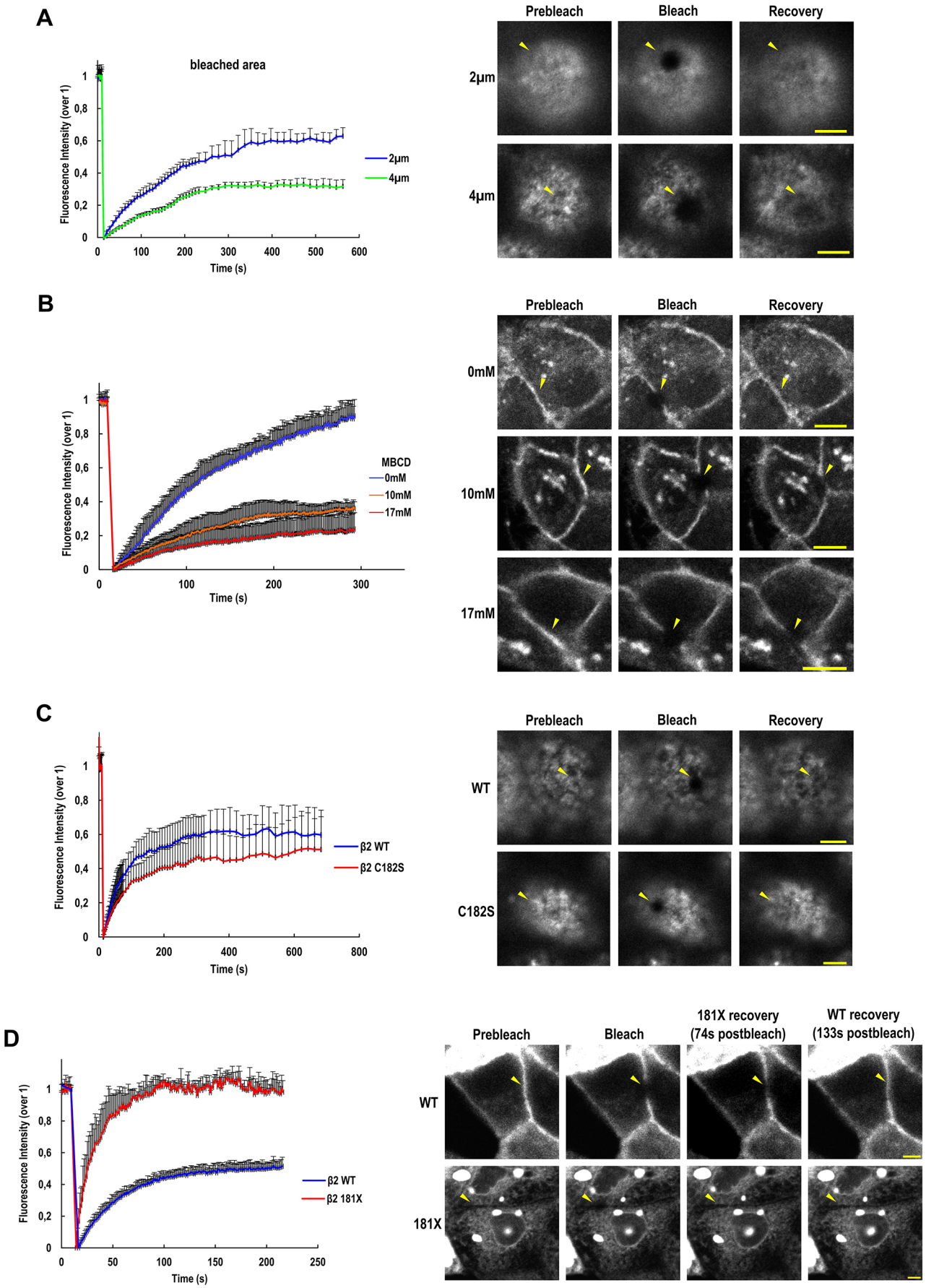

Fig. 5. See next page for legend.

Journal of Cell Science (2021) 134, jcs252189. doi:10.1242/jcs.252189

Fig. 5. Cholesterol depletion and the C182S mutation cause a decrease in the MF of β2, whereas removal of its ICD causes a dramatic increase. (A-D) Line charts of fluorescence intensity show the MF of β2 in cells stably (A,B, C) or transiently expressing β2-YFP (D), growing subconfluent for 1 (B) or 2 days (A,C,D). (A) The MF is reduced when increasing the bleached area (from r_n of 2 µm to 4 µm). (B) Increasing concentrations of MβCD dramatically reduces β2 MF. (C) The MF of β2 C182S is slightly decreased compared with that of the wild type (WT). (D) β2 181X displays considerable mobility compared with the wild type. Bleaching was performed at the upper cell section, encompassing the PM (A,C), or in a nuclear section at the cell end between two adjacent cells (B,D). Bleaching of β2 181X was performed at the cell surface to emulate the location of β2 wild type, although this mutant mainly accumulates in the ER. For each graph, images on the right show a representative cell pre-bleached, immediately after bleaching and after fluorescence recovery (arrowheads mark the bleached point). To highlight the apparent differences in MF between β2 WT and 181X, pictures of two time points are shown (D). Data are mean±s.d. Scale bars: 5 µm (A,C,D); 10 µm (B). See the complete FRAP data in Table 1.

diseases. Trafficking in polarized cells is believed to be controlled by a molecular network responsible for organizing vesicle transport to achieve the proper polarized distribution of PM proteins (Rodriguez-Boulan and Macara, 2014). In particular, preferential protein targeting to the apical domain has intrigued many scientists, and has been extensively explored. This is the case, for instance, of glycosylphosphatidylinositol-anchored proteins, which are mainly sorted to the apical surface in epithelia by partitioning into lipid rafts; these have in fact been proposed as sorting platforms for apical delivery from the trans-Golgi network (Zurzolo and Simons, 2016). Other mechanisms implicated include the recognition of the glycosylated luminal domain of proteins by sugar-binding lectins (Delacour et al., 2009).

Here, we addressed the potential relevance of palmitoylation in defining polarized trafficking and subcellular localization of β2. By protein extraction in cold non-ionic detergent, and further sucrose density-gradient ultracentrifugation, a modest, albeit measurable, fraction of β2 was recovered in DRM, which are expected to be enriched in lipid rafts (Levental et al., 2020). On the contrary, β2 C182S, with the single Cys in its ICD mutated, preventing it from being palmitoylated, was completely solubilized. This experiment suggests that only palmitoylated β2 can associate with lipid rafts. In fact, this result agrees with previous observations, as all four Na_V channel β subunits have previously been found to be enriched in DRM fractions from primary cortical neurons, supporting their preferential association with lipid raft domains (Wong et al., 2005). Their distribution may indeed be cell-type specific, as we have seen here a detergent-insoluble fraction of β2 that is comparatively smaller than that reported in neurons. Nevertheless, while our manuscript was in preparation, the first evidence of S-palmitoylation on a Na_V channel β subunit was published. Intriguingly, this report demonstrates palmitoylation of β1 at a Cys residue, conserved also in β3, which appears to promote PM localization, albeit not partitioning into lipid rafts (Bouza et al., 2020); the modification is predicted to take place in a membrane-protected domain (UniProt Consortium, 2019; see UniProtKB, Q07699). Palmitoylation on juxtamembrane regions allows inclination of the TMD. This is translated into TMD shortening, which reduces hydrophobic mismatch, i.e. it decreases the difference between TMD length and bilayer thicknesses. This seems particularly important throughout the thinner ER membrane, in which protein exit can require palmitoylation (Shipston, 2014).

Another perhaps more functionally relevant reason for the relatively small fraction of β2 wild type that we recovered in DRM could be that its traffic through DRM/Lo membrane domains, although possibly important for its apical delivery, may proceed rapidly and be short-lived, so that only a small portion of total β2 can be detected there at any given time. Moreover, it is possible that these domains can accommodate only a very small portion of β2, while all the remaining protein has already reached its location at the cell surface, or is still on its way, either in the ER or in other early steps of the exocytic pathway. Finally, we must bear in mind that the isolation of our DRM was carried out at 4°C, whereas the concept of lipid rafts applies to live cells at physiological temperature. Gel-to-fluid melting temperature of lipids influences the formation and

Table 1. FRAP data indicating that cholesterol depletion and the C182S mutation cause a decrease in the MF of β2, whereas removal of its ICD causes a dramatic increase

Bleached area (r_n, µm)	*n*	MF (%)	$\tau_{1/2}$ (s)	*D* (µm²/s)
2	3	65±2	138.0±14.4	0.002±0.000
4	3	35±2	140.7±10.7	0.007±0.001
P-value		<0.001	0.810	0.002
MβCD (mM) treatment				
0	5	89±7	94.8±21.4	0.003±0.001
20	5	39±2	106.2±39.2	0.003±0.001
35	5	23±8	93.0±47.2	0.003±0.001
P-value		<0.000 (0 vs 20 mM) <0.000 (0 vs 35 mM) 0.004 (20 vs 35 mM)	0.850	0.760
Wild type and C182S				
Wild type	17	63±8	62.8±16.5	0.004±0.001
C182S	26	52±11	79.4±24.4	0.003±0.001
P-value		<0.001	0.011	0.028
Wild type and 181X				
Wild type	3	49±3	45.5±6.61	0.006±0.001
181X	3	100±0	25.5±2.83	0.010±0.001
P-value		<0.001	0.007	0.060

Data are mean±s.d. of ≥3 experiments (*n*, total number of cells analyzed). *P*-values indicate differences calculated using an unpaired two-tailed Student's *t*-test in all cases, except for the treatment with MβCD, which was analyzed by one-way ANOVA ($\tau_{1/2}$ and *D*), or by one-way ANOVA with Tukey's honest significant difference post-hoc test (MF).

Journal of Cell Science (2021) 134, jcs252189. doi:10.1242/jcs.252189

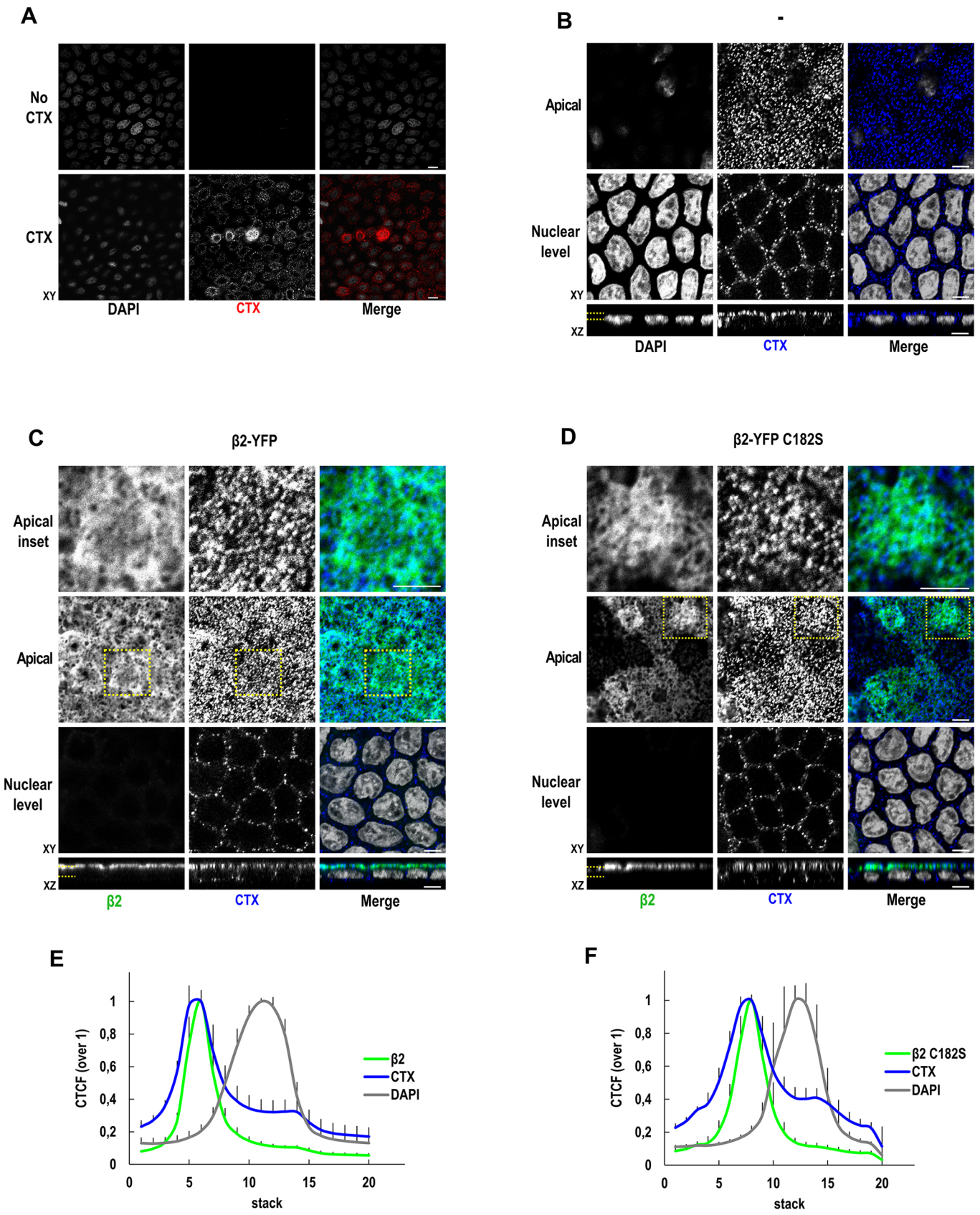

Fig. 6. See next page for legend.

Journal of Cell Science (2021) 134, jcs252189. doi:10.1242/jcs.252189

Fig. 6. Partial overlap of β2 wild type and C182S with CTX-labeled raft domains. (A-D) Representative XY sections and corresponding *z*-axis reconstructions (XZ, B-D) show surface labeling of CTX (A, red; B-D, blue) in live cells, parental (A,B), or stably expressing β2-YFP wild type (C) or C182S (D). Cells were polarized, except in A, where cells had been grown partially polarized in wells. (A) Nuclear view showing no labeling without CTX, ensuring antibody specificity, and some heterogeneous labeling intensity among cells in the presence of CTX. (B) CTX labeling is most predominantly apically, although was also present in the basolateral region. (C,D) Partial overlap of CTX with β2, either wild type or C182S, was mainly observed at the apical domain (insets). The Manders' coefficient of β2 wild type with CTX is 0.41 ±0.14, with no significant differences found with β2 C182S. The yellow dashed squares in XY indicate the inset, and the two parallel yellow dashed lines in XZ mark the sections shown by XY, either apical or nuclear. In merged images, the YFP-emitted fluorescence is in green and DAPI is in grey. Scale bars: 10 µm (A); 5 µm (B-D). (E,F) Line charts displaying the CTCF show the curve peak of apical β2, either wild type or C182S, coinciding with that of CTX and well above the nuclear level defined by DAPI.

stability of Lo and liquid-disordered domains at the membrane. As lipids with high melting temperatures are expected to be in Lo membrane domains (Bakht et al., 2007), potentially isolated by our subcellular fractionation, the presence of β2 at low temperature in these may be considerably underrepresented.

By treating cells with MβCD, which pulls cholesterol out from the PM, β2 localization was altered. Owing to their capacity to influence PM cholesterol content, cyclodextrins have been used as a tool to assess the potential influence of cholesterol-rich raft domains in protein localization and trafficking. Yet, non-specific effects may arise when they are used at high concentrations and/or for an extended period. Under such circumstances, it has been reported that these drugs remove cholesterol not only from raft regions within the PM, but also from inside the cell, which may disturb important cell functions (Zidovetzki and Levitan, 2007). To avoid non-specific effects, we thus limited the dose and incubation time of MβCD to the minimum by which β2

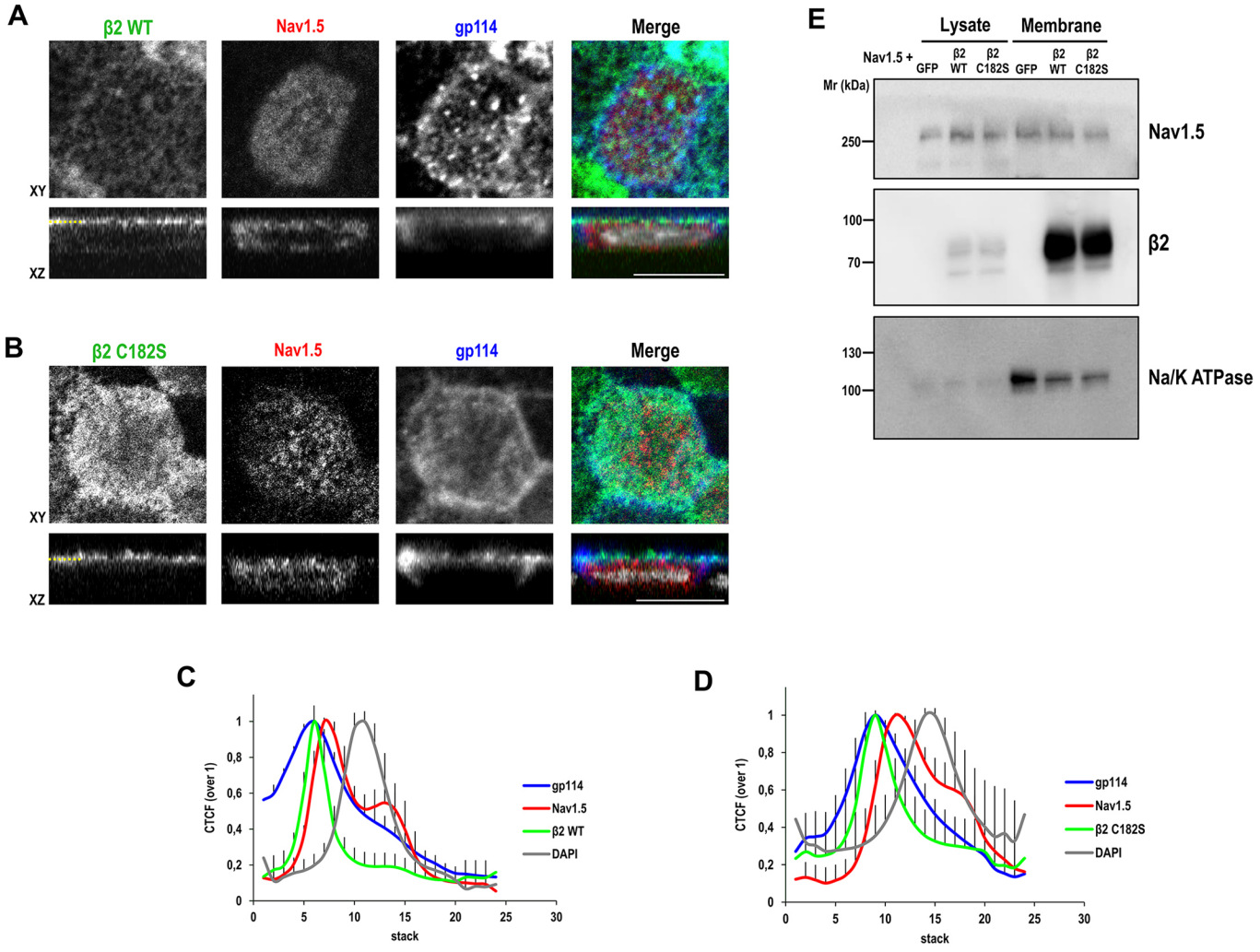

Fig. 7. β2 C182S is not defective in promoting surface localization of $Na_V1.5$. (A,B) Representative confocal XY sections and corresponding *z*-axis reconstructions (XZ) of polarized cells stably expressing β2-YFP wild type (WT) (A) or C182S (B), both transiently expressing $Na_V1.5$-FLAG, show that $Na_V1.5$ (red) is located apically, partially overlapping with gp114 (blue) and β2 (green), either with wild type (A) or C182S (B), with additional intracellular presence. The parallel yellow dashed line in XZ marks the section shown by XY. In merged images, the nuclear staining by DAPI is in grey. Scale bars: 10 µm. (C,D) Line charts displaying the CTCF show the $Na_V1.5$ curve peak close to those of apical gp114 and β2. Although with β2 C182S the $Na_V1.5$ curve slightly extends into more basal sections, with increasing overlap with DAPI (included as a reference for the nuclear level), differences with the wild type were not significant (D). (E) Representative western blots of cells stably expressing $Na_V1.5$-YFP and transiently co-expressing β2 plus $Na_V1.5$-FLAG (to ensure extensive $Na_V1.5$ overexpression) show that $Na_V1.5$ levels in recovered pulldowns (Membrane) from cells expressing β2 C182S are similar to those in cells with β2 wild type. Na/K-ATPase was blotted as a surface marker to correct for quantifications in pulldowns. Without β2 (GFP), levels of Na/K-ATPase appear higher in pulldowns. Lysates loaded in parallel correspond to one-twentieth of each sample subjected to pulldown.

Journal of Cell Science (2021) 134, jcs252189. doi:10.1242/jcs.252189

localization effectively changed, while polarity markers and the integrity of tight junctions remained unaffected.

We also analyzed potential β2 endocytosis from the apical surface. It has long been known that clathrin-coated pits are formed at the apical surface and internalized, albeit at a slower rate than from the basolateral surface (Gottlieb et al., 1993). As a positive control for apical endocytosis, we used exogenously expressed BACE1, which is present in endosomes and the trans-Golgi network and is sorted to the apical domain (Cuartero et al., 2012). As expected, a fraction of BACE1 was effectively endocytosed at an early time point. As a negative control, we used apical gp114, which is a major endogenous sialoglycoprotein regarded as non-raft associated under normal conditions (Verkade et al., 2000). If most of β2 were excluded from rafts, one would expect certain measurable endocytosis. However, no internalization could be detected, even after a long period. Once more, this suggests that the fraction of β2 that we recovered in DRM fractions may indeed be underestimated. On the other hand, potential apical β2 endocytosis, similar to the case of gp114 described previously in MDCK cells (Le Bivic et al., 1993), may be negatively influenced by its *N*-glycosylation and sialylation (Cortada et al., 2019a). These data also suggest that the mislocalization of β2 that we have observed upon cholesterol depletion is due to actual missorting to the basolateral PM, rather than to enhanced endocytosis and subsequent delivery to the basolateral surface.

By monitoring fluorescently tagged β2 by FRAP, we have analyzed the potential effect of cholesterol depletion, cytoskeleton interaction and palmitoylation abolition on its dynamics at the membrane. β2 displays a modest diffusion within the plane of the membrane (Cortada et al., 2019a). In fully polarized MDCK cells, β2 remains rather immobile; although we have seen a tendency to acquire faster mobility in cells grown on glass, the calculated *D* always remains relatively small (our unpublished observations). Therefore, the rate of β2 diffusion seems to depend on the degree of cell polarization. Moreover, the properties of the membrane and its associated structures can influence or even impede protein mobility. Thus, when the resulting *D* is of the order of 1 $\mu m^2/s$ or higher, proteins are assumed to be outside of lipid rafts; however, for a *D* of 0.05 $\mu m^2/s$ or less, more akin to our current data, they are instead believed to diffuse slowly inside lipid rafts (Pralle et al., 2000); and when *D* is below 0.001 $\mu m^2/s$, they are considered to be immobilized by cytoskeletal elements (Peran et al., 2001). According to these criteria, it is likely that a considerable fraction of β2 remains associated with the cytoskeleton; this agrees with the idea that β subunits serve as adaptors linking the cytoskeleton, along with signaling and adhesion molecules, to ion channel macromolecular complexes (Bao and Isom, 2014; Salvage et al., 2020).

Thus, the FRAP curves also provided information on how our protein of interest interacts with other membrane proteins. Curves for β2 were flat, and considerably long $\tau_{1/2}$ was extracted. This is indicative that the protein probably undergoes transient, albeit persistent, interactions with other molecules as it diffuses across the membrane (Phair and Misteli, 2001). Altogether, we propose that at least two subpopulations of β2 coexist at the PM, i.e. one anchored to the cytoskeleton by its cytoplasmic domain, and another one mobile. Most likely, a limited number of cytoskeleton-binding sites for β2 are available, generating an equilibrium between cytoskeleton-anchored (immobile) and mobile β2. The latter would undergo transient interactions with other membrane proteins, altogether also turning into discreet values of *D*. At some point, immobile β2 molecules may detach from the cytoskeleton to become mobile. In support of this model, we provide the data for β2 lacking its ICD (181X); this mutant displayed considerably faster mobility than the wild type and a complete fluorescence recovery, most likely due to its defective interaction with the submembrane cytoskeleton.

The mobility of β2 was also greatly reduced upon acute (short-term) cholesterol depletion. This decrease in mobility is consistent with the idea that cholesterol depletion affects raft-associated proteins, as seen in previous studies (Agarwal et al., 2014; Marlar et al., 2014). However, MβCD treatment also appears to reduce the diffusion of non-raft membrane proteins, suggesting that it may cause some effects independent of membrane cholesterol content (Shvartsman et al., 2006). Nevertheless, the distribution of polarity markers during our acute treatment was not altered, suggesting that the conditions used specifically affected β2. In addition, the palmitoylation-deficient mutant also displayed reduced mobility in control conditions. Thus, our data support the notion that a measurable fraction of β2 is associated with cholesterol-enriched raft domains at the cell surface.

Why was the mobility of β2 C182S only mildly reduced? It is quite possible that the fraction of the palmitoylation-deficient mutant with a decreased MF actually corresponds to the equivalent portion of the wild type that becomes palmitoylated at steady state in cells; this relatively small portion would agree with the modest presence of β2 wild type that we found in DRM fractions. Even though DRM do not necessarily correspond to lipid rafts, they are rich in sphingolipids and cholesterol, as described for rafts. Although finding a molecule in DRM fractions does not provide conclusive evidence of its localization in rafts, cold detergent-extraction is still considered a useful tool for studying membrane biology (Levental et al., 2020). To further investigate the likely association of β2 with lipid raft domains, we labeled polarized live cells with CTX, the B subunit of which binds to lipid raft-associated GM1 (Janich and Corbeil, 2007). Here, we observed a partial overlap of β2 with CTX. Altogether, our data show that a fraction of β2 is associated with Lo membrane regions, which can be considered as cholesterol-enriched raft domains.

It may seem surprising to have found β2 C182S also overlapping with CTX. However, the outcome of these experiments – which we performed in live cells, using an anti-CTB antibody to force crosslinking of the CTX-labeled lipid rafts, and also by labeling previously fixed cells with CTX – may be subject to misjudgment due to technical limitations. Firstly, endogenous expression of GM1 in MDCK cells, to which CTX specifically binds, is said to be very low, yet the ganglioside effectively localizes apically upon transfection of the right galactosyltransferase (Crespo et al., 2008). In fact, we have observed that CTX binds to the apical surface very unevenly, with some strongly positive regions of the monolayer amidst large negative areas. A second important limitation is that the conventional confocal microscope used cannot resolve discrete raft domains, and therefore the images that we present are the best approximation that we could possibly achieve with our instrument.

Finally, we wondered about the potential functional consequences of β2 palmitoylation on $Na_V1.5$. Our previous data support the model that associated β2 subunits fulfill their role within the Na_V channel mainly by promoting cell surface expression of the α subunit. As β2 C182S appeared similarly effective to β2 wild type in promoting the localization of $Na_V1.5$ to the PM, we conclude that, β2 palmitoylation is not implicated in chaperoning $Na_V1.5$ on its way to the cell surface. According to our results, one could thus assume that as long as the associated β subunit efficiently reaches the PM, which would be the apical domain in MDCK cells, there would be no detectable defect in

Journal of Cell Science (2021) 134, jcs252189. doi:10.1242/jcs.252189

bringing $Na_V1.5$ along. A remarkable example of this would be, as we previously found, that a single glycosylation site in β2 is sufficient to allow its trafficking to the apical surface and, as a result, to promote surface localization of $Na_V1.5$ (Cortada et al., 2019a), although there may be exceptions, as we saw with Brugada syndrome-associated β2 D211G (Dulsat et al., 2017).

The lack of an obvious defect with the localization of $Na_V1.5$ in the presence of β2 C182S also suggests that the role of β2 within the channel may be subtle, and probably more complex than what we have analyzed here. Thus, gating effects of β2 on $Na_V1.5$ were demonstrated several years ago, and were caused by β2 sialylation, potentially because of the influence of its negative charged sialic acids on *N*-linked glycans of the α subunit (Johnson and Bennett, 2006). On the other hand, there is increasing evidence that β subunits, perhaps including β2, participate in trans-heterophilic interactions to promote cellular adhesion in the adjacent perinexal membranes, which may influence local clustering, and thereby the functioning of $Na_V1.5$ (Salvage et al., 2020). Interestingly, the reported palmitoylation-deficient β1 was as effective as the wild type in modulating sodium current density (Bouza et al., 2020), which agrees with the outcome with β2 C182S. Nevertheless, palmitoylation of β2 may still have important implications in regulating its association within lipid raft domains and its polarized localization to the cell surface. Additional elements, perhaps only present in cardiomyocytes and/or other excitable cells, may participate in interactions between β2 and Nav1.5, thereby revealing potential effects, as well as the consequent defects, due to mutations in β subunits.

In summary, we provide evidence that β2 is palmitoylated, which would increase its affinity for DRM, thereby giving support to the notion that it is present in lipid rafts. Moreover, cholesterol depletion dramatically affected β2 polarized localization. The C182S mutation abrogates palmitoylation of the single available cysteine in the β2 ICD. Yet, we found that β2 C182S properly localizes to the apical PM in a manner indistinguishable to the wild type, and that its subcellular distribution is also sensitive to cholesterol depletion. Thus, palmitoylation by itself does not determine apical localization of β2, although it may contribute to its partition into raft subdomains potentially important to establish its polarized distribution. In this regard, β2 localization within membrane subdomains may also be affected by the nature of its TMD, and possibly be regulated by its length (Sharpe et al., 2010). Importantly, understanding how β2 trafficking is regulated will add to our knowledge about how it influences the subcellular localization of $Na_V1.5$.

MATERIALS AND METHODS

Plasmid vectors, cDNA cloning and site-directed mutagenesis

The vector containing *SCN2B-yfp*, to express β2 with YFP fused to its C-terminus (Dulsat et al., 2017), the vector to express human BACE1 (Capell et al., 2000), and the vector comprising FLAG-tagged human *SCN5A* cloned in pcDNA3.1 (Valdivia et al., 2010), have all been described previously. Following the manufacturer's instructions, the QuikChange Lightning Site-Directed Mutagenesis Kit (Agilent Technologies, Inc., Santa Clara, CA, USA) was used to change Cys-182 to Ser (changing to Ser intends to avoid affecting the protein's tertiary structure). This single Cys residue in the ICD of β2 is conserved among vertebrates (Chopra et al., 2007), and in humans corresponds to the second residue after its predicted TMD (UniProt Consortium, 2019; see UniProtKB, O60939). Both vectors with *SCN2B-yfp* and *SCN2B-cfp* were made to express β2 C182S.

Human *SCN2B* (Consensus Coding Sequence database 8390.1), containing the desired mutation, was used as a template. Complementary primer pairs for PCR were designed using the QuikChange Primer Design Program (Agilent) and synthesized by Metabion International AG (Steinkirchen, Bavaria, Germany). Sequences were as follows: 5′-GTGCTGATGGTGGTCAAG**A**GTGTGAGGAGAAAAAAAG-3′ (sense) and 5′-CTTTTTTCTCCTCACAC**T**CTTGACCACCATCAGCAC-3′ (antisense); mutated bases are marked in bold and underlined.

To generate a tail-minus β2-YFP, the same method was applied but using the following primer pairs to remove the ICD, equivalent to amino acids 182-215: 5′-GCTGATGGTGGTC–GCGGCCGCGATGG-3′ (sense) and 5′-CCATCGCGGCCGC–GACCACCATCAGC-3′ (antisense); the location of the sequence removed is indicated with a dash. As β2 lacking the ICD (181X) was poorly expressed, we added a $(Gly\text{-}Gly\text{-}Ser\text{-}Gly)_2$ linker between residue 181 and the YFP tag using the following primer pairs: 5′-GCTGATGGTGGTC**GGTGGTTCTGGTGGTGGTTCTGGT**GCGG-CCGCGATGG-3′ (sense) and 5′-CCATCGCGGCCGC**ACCAGAACC-ACCACCAGAACCACC**GACCACCATCAGC-3′ (antisense); introduced bases are marked in bold and underlined. All constructs were verified by sequencing.

Cell culture and transient transfection

MDCK cells II and transfectant derivatives were maintained in minimum essential medium (MEM) with Earl's salts, supplemented with 10% fetal bovine serum and 1% GlutaMAX (Gibco, Thermo Fisher Scientific, Waltham, MS, USA); cells had been validated and tested for contamination. To generate a fully polarized monolayer, cells were grown on 12 mm-diameter polycarbonate Transwell filters with 0.4 µm pore size for at least 3 days (Corning, NY, USA), as described previously (Verges et al., 2007). Transfections were performed, following the manufacturer's instructions, with Lipofectamine 2000 in Gibco Opti-MEM I reduced-serum medium (Invitrogen, Thermo Fisher Scientific), as described previously (Cortada et al., 2019a). Briefly, cells were seeded and immediately transfected, in suspension, with plasmid DNA to express β2 with 1 µl transfection reagent per µg DNA; in general, 400,000 cells and 2 µg DNA were used per Transwell, whereas 1.2×10^6 cells were used per 35-mm well (six-well plates). Specifically, 3 µg *SCN5A*-FLAG vector was transfected into β2 stable cells in Transwells (800,000 cells), but 2 µg *SCN5A*-FLAG plus 3 µg *SCN2B*-yfp vectors were used for cells in 35-mm wells. In $Na_V1.5$/β2 co-transfections, the pEGFP-N1 vector [Clontech Laboratories (now Takara Bio USA), Kyoto, Japan] was used as a control for β2-YFP. For FRAP experiments, 180,000 cells were seeded on ibidi µ-slides, with four wells Ph^+ and a glass bottom, and transfected with 1.5 µg DNA.

Generation of stable cell lines

Transfections were performed by calcium phosphate co-precipitation, as described previously (Breitfeld et al., 1989), and single-cell clones were then selected with 200 µg/ml G418 (Sigma–Merck, Darmstadt, Hesse, Germany). Positive clones for CFP- or YFP-tagged β2 – wild type, C182S and 181X – were visually identified using the appropriate filter under a fluorescence microscope, and then confirmed by western blot to β2 or GFP. Proper distribution of cell surface markers (apical gp114 and basolateral p58) and tight junctions (ZO-1) was then verified by immunofluorescence, ensuring normal cell polarity.

Isolation of detergent-resistant membranes

The following procedure has been described previously (Reverter et al., 2011), but was slightly modified here. The procedure was entirely performed at 4°C, and buffers were supplemented with a cocktail of protease inhibitors. Confluent cells – 4×10-cm dishes per condition – were homogenized in 20 mM HEPES/NaOH (pH 7.4), containing 1 mM EDTA and 250 mM sucrose (4 ml in total), by 30 passages through a 22-gauge needle. The homogenate was centrifuged at 255,000 ***g*** for 90 min in a Beckman MLA-130 rotor (Beckman Coulter, Brea, CA, US). The pellet was then resuspended in 1 ml MOPS-buffered saline (MBS) [25 mM MOPS/NaOH (pH 6.5) with 150 mM NaCl], containing 1% Triton X-100, and left on ice for 20 min. This solubilized material was then resuspended with 30 passages through a 22-gauge needle and mixed with an equal volume of 90% sucrose (w/v, in H_2O), which was then overlaid with 35% sucrose (2 ml) and 5% sucrose (1 ml), both

prepared in detergent-free MBS. Samples were centrifuged at 235,000 ***g*** overnight in a Beckman SW 55 Ti Rotor. Approximately ten fractions were collected (0.5 ml each) from top to bottom. The upper 2 to 3 fractions are those that are detergent-insoluble and thus defined as DRM.

Normalized abundance of each protein in the isolated fractions was performed by quantifying the intensity of blotted protein bands from each fraction and plotting relative band intensity, i.e. over 1, giving the value of '1' to that obtained in the fraction with the maximum band intensity. The relative portion of β2 within DRM was estimated by determining the ratio between the added intensity of bands within the DRM fractions over the total intensity of β2 bands in all fractions collected. Three experiments were analyzed.

Pharmacological depletion of cholesterol

In all treatments, cells were first rinsed twice with warm Dulbecco's PBS^+ ($DPBS^+$; i.e. DPBS containing divalent cations), and the corresponding drug was added in Opti-MEM, which lacks cholesterol and lipoproteins, thus preventing cells from obtaining exogenous cholesterol. In untreated controls, an equivalent volume of the drug solvent was added.

Cells were treated for 1 h with 5 mM MβCD (Sigma-Aldrich, 332615) to acutely deplete cell surface cholesterol (Zidovetzki and Levitan, 2007). MβCD was dissolved directly in Opti-MEM and prepared fresh; the dose and time of incubation were previously titrated by ensuring the absence of non-specific effects in the localization of cell surface markers.

In some experiments, cells were treated for 24 h with U18666A (Sigma-Aldrich, U3633) to inhibit intracellular cholesterol transport (Cenedella, 2009). U18666A was added at the indicated concentration from a stock solution at 10 mg/ml in DMSO, previously aliquoted and stored at −20°C.

To inhibit cholesterol synthesis (Alberts, 1988), cells were pretreated overnight in some experiments with lovastatin (also known as mevinolin, Sigma-Aldrich, PHR1285) at the indicated concentration, prepared from a stock solution, as follows. Hydrolysis of its lactone ring to get the β-hydroxy acid (open-ring) form (i.e. the active form) was performed in ethanolic NaOH, as described previously (Fenton et al., 1992). Briefly, lovastatin was first dissolved at 40 mg/ml in ethanol. Then, 0.1 N NaOH at 1.5-fold the volume of ethanol was added, and the mixture was heated for 2 h at 50°C. The solution was rapidly cooled on ice until it reached room temperature, and the pH was then adjusted to 7.2 with HCl. It was then brought to tenfold the initial volume of ethanol with sterile H_2O. The resulting solution (4 mg/ml, i.e. 10 mM) was aliquoted and stored at −20°C.

In vitro deglycosylation

To discern between simple and complex *N*-glycosylation, we used Endo H (P0702; New England Biolabs, Ipswich, MA, USA), which cleaves *N*-glycans on high-mannose and hybrid, but not complex, glycans. Deglycosylation was performed in whole-cell lysates as described previously (Cortada et al., 2019a). Briefly, 7.5 µg of protein was denatured for 10 min at 100°C in 10 µl glycoprotein denaturing buffer (0.5% SDS with 40 mM DTT). The reaction with 1 µl Endo H (500 units) was then performed in a total volume of 20 µl, including GlycoBuffer 3 (50 mM sodium acetate at pH 6), by overnight incubation at 37°C. Reactions were stopped with Laemmli buffer.

Antibodies

Some antibodies were provided by other researchers and have been described previously. These include the rabbit polyclonal antibodies 7523 to BACE1 (Capell et al., 2000) and 786 to VPS26A (Haft et al., 2000), the mouse monoclonal antibodies to gp114 (a cell adhesion molecule) and to p58 (the Na/K-ATPase β subunit) (Fullekrug et al., 2006), and the rat monoclonal antibody against ZO-1 (Stevenson et al., 1986). The following antibodies are commercially available mouse monoclonal antibodies: anti-flotillin-1 (BD 610820; BD Transduction Laboratories, Franklin Lakes, NJ, USA) and the anti-Na/K-ATPase α1 subunit (Abcam, ab7671). Commercial rabbit polyclonal antibodies used were: anti-β2 (ASC-007; Alomone Labs, Jerusalem, Israel), anti-caveolin-1 (BD 610060), anti-CTB (from the Vybrant Lipid Raft Labeling Kit, Molecular Probes V-34405), anti-biotin (Abcam, ab53494) and anti-GFP (Abcam, ab290). Primary antibodies were used at a dilution of 0.5-1 µg/ml of purified IgG for western blot and fivefold to tenfold more concentrated for immunofluorescence.

Horseradish peroxidase-conjugated secondary antibodies for western blot were obtained from Jackson ImmunoResearch (111-035-003 and 115-035-003), and Alexa Fluor-labeled secondary antibodies for immunofluorescence were obtained from Molecular Probes [all raised in goat; excitation peak (Ex), 488 nm, anti-rabbit IgG A-11008; Ex 594 nm, anti-mouse IgG A-11005 and anti-rabbit IgG A-11012; Ex 633 nm, anti-rabbit A-21070 and anti-rat A-21094].

Sample preparation, western blot and quantitation of protein band intensity

Protein determination of cell lysates, sample preparation for SDS-PAGE and western blot, and subsequent stripping for antibody reprobing, were performed essentially as described previously (Dulsat et al., 2017), with slight modifications, as follows. Samples were prepared in Laemmli buffer by heating at 95°C for 5 min, and protein transfer to PVDF membranes was performed overnight without SDS. Detection of blotted protein bands was carried out by enhanced chemiluminescence (Thermo Fisher Scientific), followed by visualization in a ChemiDoc MP Imaging System (Bio-Rad, Hercules, CA, USA). Band intensities were quantified using the Public Domain ImageJ platform. In all figures displayed, molecular weight (Mr) markers are in kDa.

Protein from DRM fractions was concentrated by precipitation with trichloroacetic acid (TCA, Sigma-Aldrich, T6399), as follows. To a given volume of each collected fraction, containing an identical amount of protein, e.g. 6 µg, one-tenth of a 100% (w/v) TCA solution was added (previously prepared by dissolving 220 g TCA in 100 ml H_2O). After vigorous vortex, the mixture was left on ice for 10 min and microfuged at maximum speed at 4°C. After removing the supernatant, 1 ml acetone at −20°C was added, without loosening up the pellet, and spun again. The pellet was then allowed to dry, dissolved in Laemmli buffer and processed as above, ensuring that it reached an adequate pH for SDS-PAGE by adding, if required, 1 µl 1 M Tris/HCl at pH 8.8.

Cell surface biotinylation

Surface protein biotinylation was performed at 4°C with EZ-Link Sulfo-NHS-SS-Biotin (Thermo Fisher Scientific, 21441), a water-soluble and membrane impermeable reagent. The procedure that was followed has been described previously in detail (Cuartero et al., 2012; Dulsat et al., 2017). Cells growing in Transwells were biotinylated either at the apical or basolateral surface. The same amount of protein was used to process each cell lysate (~200 µg, unless otherwise specified), and nine-tenths of it was subjected to overnight pulldown with NeutrAvidin (Thermo Fisher Scientific, 53150). Pulldowns and lysates were analyzed by western blotting and quantification of blotted protein bands was performed as described previously (Dulsat et al., 2017).

To examine apical endocytosis of β2, we proceeded as previously described (Cuartero et al., 2012). Briefly, the apical surface of cells growing in Transwells was biotinylated. We then examined endocytosis for various time periods at 37°C by glutathione cleavage of surface-exposed biotinylated proteins. By reducing the disulfide bond of the biotin reagent, glutathione removes the biotin tags from labeled membrane proteins. As it does not permeate into cells, intracellular biotin moieties of endocytosed proteins remain protected, and are then detected by western blot. An additional Transwell was left untreated, representing at time zero the total amount of biotin reagent bound to surface proteins.

Acyl-Biotin exchange assay

Detection of protein S-acylation (which we will refer to here as palmitoylation, as the most common form of S-acylation) was performed by immunoprecipitation and ABE. A total of 400,000 cells/35-mm well (six-well plates) were seeded and allowed to grow until confluence for 3 days. Immunoprecipitation was essentially performed as described previously (Dulsat et al., 2017). Here, cells were lysed at 4°C with 1% (w/v) IGEPAL CA-630 (formerly Nonidet P-40) in 20 mM HEPES/NaOH (pH 7.2) containing 150 mM NaCl; all buffers were prepared fresh and supplemented with a protease inhibitors cocktail. The same amount of protein was used to process each cell lysate (~300 µg), and nine-tenths of the protein was subjected to immunoprecipitation. To ensure exhaustive blocking of free

sulfhydryl groups (thiols), 50 mM NEM (Thermo Fisher Scientific, 23030) was included, essentially as described previously (Drisdel and Green, 2004). Immunoprecipitation of β2-YFP was performed for at least 1 h with an anti-GFP antibody previously conjugated to Protein A-agarose beads (Thermo Fisher Scientific, 15918-014) at 0.5 µg IgG per sample. Extensive washing of immunoprecipitates at 4°C was required to ensure the total removal of residual NEM, as described previously (Wan et al., 2007). Next, cleavage of the acyl-thioester bond with 1 M HAM·HCl (Thermo Fisher Scientific, 26103) in DPBS containing 0.2% Triton X-100 was performed for 1 h at room temperature after adjusting the pH to 7.2 with NaOH. Then, the free sulfhydryl residues generated were specifically labeled with EZ-Link BMCC-Biotin (Thermo Fisher Scientific, 21900) at 40 µM in DPBS, previously adjusted to pH 7.0 with HCl, for 2 h at room temperature; an 8 mM stock solution of BMCC-Biotin in DMSO was prepared immediately before use. Finally, beads were washed, and immobilized proteins were eluted in Laemmli buffer and then analyzed by western blotting to detect biotinylated (acylated) and total β2 in immunoprecipitates.

Various controls were performed. First, NEM was not included. Without NEM, several non-specific bands appeared as a result of the presence of free unblocked thiol groups in proteins that were subsequently biotinylated and detected; when NEM was included in immunoprecipitations, such bands were absent. Second, HAM cleavage was omitted in one-half of each immunoprecipitate. Without HAM, palmitoyl chains are not removed and their otherwise free thiols cannot be biotinylated and detected; this serves as a control for potential contaminants of the immunoprecipitation and for unspecific biotinylation (an equivalent amount of antibody alone was processed in parallel in the presence of HAM). Third, as a negative control for palmitoylation, an irrelevant, not palmitoylated, protein was immunoprecipitated, and the sample subjected in parallel to ABE; we chose VPS26A, which is enriched in the endosomal compartment of MDCK cells (Mellado et al., 2014). And fourth, metabolic labeling with the palmitate analog 2-BP (Sigma-Aldrich, 238422) was performed to inhibit palmitoylation in cells. Before the experiment, cells were grown for 1 h in medium containing 2% serum, and 2-BP was added at increasing concentrations (within the µM range, from a 100 mM stock prepared fresh in ethanol) and left for 1 h more; an equivalent volume of solvent was added in untreated controls.

The normalized palmitoylation signal was obtained by plotting relative quantified band intensities, i.e. the ratio between the intensity detected with the antibody to biotin over the corresponding β2 signal. The value of '1' was given to the ratio obtained in the absence of HAM for each ±HAM pair, that is, for each condition.

Fluorescent labeling of membrane lipid rafts with cholera toxin

Two different approaches were followed. In the first approach, live cells were incubated with 10 µg/ml CTX (Sigma-Aldrich, C8052) for 10 min in complete medium at 4°C; CTB binds to the lipid raft-associated ganglioside GM1 (Janich and Corbeil, 2007). After extensive rinsing with ice-cold medium, cells were incubated at 4°C with an anti-CTB antibody (at 1:200) for 15 min in complete medium to cluster bound CTX. After extensive rinsing with ice-cold DPBS$^+$, cells were fixed at room temperature with 4% paraformaldehyde for 20 min. Then, we proceeded with a 30 min incubation with an Alexa Fluor-labeled secondary antibody in complete medium at room temperature, nuclei staining with DAPI and mounting of the slide for fluorescence microscopy analysis, as described previously (Cuartero et al., 2012).

In the second approach, clustering of bound CTX was not induced. Here, cells were first fixed and then labeled with CTX, as above, but for 30 min in DPBS$^+$ containing 0.025% saponin and 0.7% fish skin gelatin. Cells were then incubated overnight at 4°C with primary antibodies anti-CTB and against apical gp114 for subsequent fluorescence microscopy analysis, as described previously (Cuartero et al., 2012). All images displayed were taken using a confocal microscope, except when verifying the specificity of the anti-CTB antibody, taken by epifluorescence.

Confocal immunofluorescence microscopy and quantitative image analysis

Cells were grown polarized in Transwells, fixed with paraformaldehyde and immunostained, essentially as described previously (Cuartero et al., 2012). High magnification images were taken using a Nikon A1R confocal microscope at a minimum pixel resolution of 1024×1024, using the NIS-Elements AR software (Nikon), as described previously (Mellado et al., 2014). Images were exported to TIFF format and colocalization was assessed without image preprocessing using Fiji, the ImageJ-based package that includes the JACoP plug-in. Manders' colocalization coefficients were then calculated to estimate the fraction of β2 present in CTX$^+$ compartments, as described previously (Dulsat et al., 2017). Eight images were analyzed.

To measure cell fluorescence along *z*-stacks (optical slice thickness of 0.5 µm), confocal images were taken at 512×512-pixel resolution. As previously described (Mellado et al., 2014), we calculated the CTCF along three-dimensional reconstructions. The CTCF, which integrates fluorescence intensity and area, was displayed in line charts along apical-to-basal *z*-stacks or sections (1, most apical section) and presented over 1, giving the value of '1' to that obtained in the section with maximum intensity. Ten cells were analyzed per condition.

Fluorescence recovery after photobleaching

Dynamics of fluorescently tagged β2 was monitored by FRAP. Cells, transiently or stably expressing β2-YFP, were grown subconfluent (1 or 2 days, as indicated) on ibidi glass supports. Cells were placed in a live-cell imaging chamber at 37°C and 5% CO_2, and imaged through a water immersion objective (Plan-Apo 60X, 1.2 NA) on a Nikon A1R confocal microscope, as described previously (Cortada et al., 2019a), with two specific details. First, the pinhole radius was always set to 3 Airy units, and second, r_n of bleached and non-bleached (reference) areas was 2 µm, except when otherwise indicated.

For treatment with MβCD, and before the experiment, cells were preincubated for 10 min with increasing concentrations of the drug in Opti-MEM. FRAP analyses were then performed in the presence of MβCD for up to an additional 30 min. In this case, and also when comparing dynamics of β2-YFP wild type with 181X, images were collected at a rate of 1 frame per second, as described previously (Cortada et al., 2019a). When comparing dynamics of the wild type with C182S, post-bleaching images were captured for 1 min at 1 frame each 2 s; then, for 4 min at 1 frame each 8 s; and subsequently, at 1 frame each 20 s, until fluorescence recovery had reached a plateau. Finally, when comparing bleached area, post-bleaching images were captured for 1 min at 1 frame each 7 s, and at 1 frame each 15 s until reaching the plateau. We used the NIS-Elements AR software (Nikon) for fluorescence intensity measurement and data correction, as previously described (Cortada et al., 2019a).

Normalization of the data was performed as previously described (Cortada et al., 2019a). From each curve of fluorescence intensity (represented over '1', i.e. the intensity before bleaching), we obtained: (1) the MF, which indicates the portion of molecules that can undergo diffusion during the experiment; (2) the $\tau_{1/2}$, i.e. the time-point in which half of total fluorescence recovery has occurred; and (3) the *D*, indicating rate of diffusion, and described fluorescence by applying the simplified Soumpasis equation (Kang et al., 2012):

$$D = 0.25 \times (r_n^2/\tau_{1/2}).$$

Statistics

All experiments were performed a minimum of three times. Data are mean± s.d., and displayed as curves or bar graphs superimposed to scatter plots, showing all the individual data points. Statistical significance was calculated using an unpaired two-tailed Student's *t*-test. Alternatively, we applied one-way ANOVA with Tukey's honest significant difference or Dunnett's post hoc tests, using the R software for statistical computing (Dessau and Pipper, 2008), when differences among groups needed to be tested. *P*-values are specified in figure legends.

Acknowledgements

DNA constructs that express β2-YFP and BACE1 were kindly donated by Thomas Zimmer and Anja Capell, respectively. Antibodies against gp114 and p58, ZO-1, VPS26A, and BACE1 were kindly donated by Kai Simons, Bruce R. Stevenson, Juan Bonifacino and Anja Capell, respectively. We thank Maria Goetz, Irene Pulido,

Montserrat Colomo and Martina Vila for contributing to this project as undergraduate students. We appreciate the service and advice from the technicians at the confocal microscopy facility in the University of Girona Research Technical Services, and from Maria Buxó (IDIBGI Statistical Service). We also thank Carlos Enrich and Carles Rentero for their helpful comments and for allowing us to use their lab space and equipment to perform cell fractionation at the University of Barcelona. We also thank the Spanish Instituto de Salud Carlos III (ISCIII); the CIBERCV is an initiative of the ISCIII from the Spanish Ministerio de Ciencia, Innovación y Universidades.

Competing interests
The authors declare no competing or financial interests.

Author contributions
Conceptualization: E.C., M.V.; Methodology: E.C., R.S.; Validation: E.C., R.S., M.V.; Formal analysis: E.C.; Investigation: E.C., R.S.; Resources: R.B., M.V.; Data curation: E.C., R.S., M.V.; Writing - original draft: M.V.; Writing - review & editing: E.C., M.V.; Visualization: E.C., R.S., M.V.; Supervision: M.V.; Project administration: R.B.; Funding acquisition: R.B., M.V.

Funding
This study was supported by the Fundación Bancaria Caixa d'Estalvis i Pensions de Barcelona (to R.B.), and from the crowdfunding platform Precipita, endorsed by the Fundación Española para la Ciencia y la Tecnología (FECYT) (PR220 to M.V. and E.C.). E.C. was a recipient of a predoctoral fellowship (FI_B 00071) from the Agència de Gestió d'Ajuts Universitaris i de Recerca (AGAUR) of the Generalitat de Catalunya, co-financed by the European Social Fund.

Supplementary information
Supplementary information available online at
https://jcs.biologists.org/lookup/doi/10.1242/jcs.252189.supplemental

Peer review history
The peer review history is available online at
https://jcs.biologists.org/lookup/doi/10.1242/jcs.252189.reviewer-comments.pdf

References
Agarwal, S. R., Yang, P.-C., Rice, M., Singer, C. A., Nikolaev, V. O., Lohse, M. J., Clancy, C. E. and Harvey, R. D. (2014). Role of membrane microdomains in compartmentation of cAMP signaling. *PLoS ONE* **9**, e95835. doi:10.1371/journal.pone.0095835

Aicart-Ramos, C., Valero, R. A. and Rodriguez-Crespo, I. (2011). Protein palmitoylation and subcellular trafficking. *Biochim. Biophys. Acta (BBA) Biomembr.* **1808**, 2981-2994. doi:10.1016/j.bbamem.2011.07.009

Alberts, A. W. (1988). Discovery, biochemistry and biology of lovastatin. *Am. J. Cardiol.* **62**, J10-J15. doi:10.1016/0002-9149(88)90002-1

Amin, A. S., Asghari-Roodsari, A. and Tan, H. L. (2010). Cardiac sodium channelopathies. *Pflügers Arch. Eur. J. Physiol.* **460**, 223-237. doi:10.1007/s00424-009-0761-0

Bakht, O., Pathak, P. and London, E. (2007). Effect of the structure of lipids favoring disordered domain formation on the stability of cholesterol-containing ordered domains (lipid rafts): identification of multiple raft-stabilization mechanisms. *Biophys. J.* **93**, 4307-4318. doi:10.1529/biophysj.107.114967

Balse, E., Steele, D. F., Abriel, H., Coulombe, A., Fedida, D. and Hatem, S. N. (2012). Dynamic of ion channel expression at the plasma membrane of cardiomyocytes. *Physiol. Rev.* **92**, 1317-1358. doi:10.1152/physrev.00041.2011

Bao, Y. and Isom, L. L. (2014). Nav1.5 and regulatory β subunits in cardiac sodium channelopathies. *Card. Electrophysiol. Clin.* **6**, 679-694. doi:10.1016/j.ccep.2014.07.002

Bao, Y., Willis, B. C., Frasier, C. R., Lopez-Santiago, L. F., Lin, X., Ramos-Mondragón, R., Auerbach, D. S., Chen, C., Wang, Z., Anumonwo, J. et al. (2016). Scn2b deletion in mice results in ventricular and atrial arrhythmias. *Circ. Arrhythm. Electrophysiol.* **9**, e003923. doi:10.1161/CIRCEP.116.003923

Bouza, A. A., Philippe, J. M., Edokobi, N., Pinsky, A. M., Offord, J., Calhoun, J. D., Lopez-Florán, M., Lopez-Santiago, L. F., Jenkins, P. M. and Isom, L. L. (2020). Sodium channel β1 subunits are post-translationally modified by tyrosine phosphorylation, S-palmitoylation, and regulated intramembrane proteolysis. *J. Biol. Chem.* **295**, 10380-10393. doi:10.1074/jbc.RA120.013978

Brackenbury, W. J. and Isom, L. L. (2011). Na^+ channel β subunits: overachievers of the ion channel family. *Front. Pharmacol.* **2**, 53. doi:10.3389/fphar.2011.00053

Breitfeld, P. P., Casanova, J. E., Harris, J. M., Simister, N. E. and Mostov, K. E. (1989). Expression and analysis of the polymeric immunoglobulin receptor in Madin—Darby canine kidney cells using retroviral vectors. *Methods Cell Biol.* **32**, 329-337. doi:10.1016/S0091-679X(08)61178-4

Capell, A., Steiner, H., Willem, M., Kaiser, H., Meyer, C., Walter, J., Lammich, S., Multhaup, G. and Haass, C. (2000). Maturation and pro-peptide cleavage of β-secretase. *J. Biol. Chem.* **275**, 30849-30854. doi:10.1074/jbc.M003202200

Cenedella, R. J. (2009). Cholesterol synthesis inhibitor U18666A and the role of sterol metabolism and trafficking in numerous pathophysiological processes. *Lipids* **44**, 477-487. doi:10.1007/s11745-009-3305-7

Chen, C., Bharucha, V., Chen, Y., Westenbroek, R. E., Brown, A., Malhotra, J. D., Jones, D., Avery, C., Gillespie, P. J., III, Kazen-Gillespie, K. A. et al. (2002). Reduced sodium channel density, altered voltage dependence of inactivation, and increased susceptibility to seizures in mice lacking sodium channel β2-subunits. *Proc. Natl. Acad. Sci. USA* **99**, 17072-17077. doi:10.1073/pnas.212638099

Chen, C., Calhoun, J. D., Zhang, Y., Lopez-Santiago, L., Zhou, N., Davis, T. H., Salzer, J. L. and Isom, L. L. (2012). Identification of the cysteine residue responsible for disulfide linkage of Na^+ channel α and β2 subunits. *J. Biol. Chem.* **287**, 39061-39069. doi:10.1074/jbc.M112.397646

Chopra, S. S., Watanabe, H., Zhong, T. P. and Roden, D. M. (2007). Molecular cloning and analysis of zebrafish voltage-gated sodium channel beta subunit genes: implications for the evolution of electrical signaling in vertebrates. *BMC Evol. Biol.* **7**, 113. doi:10.1186/1471-2148-7-113

Cortada, E., Brugada, R. and Verges, M. (2019a). N-Glycosylation of the voltage-gated sodium channel β2 subunit is required for efficient trafficking of NaV1.5/β2 to the plasma membrane. *J. Biol. Chem.* **294**, 16123-16140. doi:10.1074/jbc.RA119.007903

Cortada, E., Brugada, R. and Verges, M. (2019b). Trafficking and function of the voltage-gated sodium channel β2 subunit. *Biomolecules* **9**, 604. doi:10.3390/biom9100604

Crespo, P. M., von Muhlinen, N., Iglesias-Bartolomé, R. and Daniotti, J. L. (2008). Complex gangliosides are apically sorted in polarized MDCK cells and internalized by clathrin-independent endocytosis. *FEBS J.* **275**, 6043-6056. doi:10.1111/j.1742-4658.2008.06732.x

Cuartero, Y., Mellado, M., Capell, A., Álvarez-Dolado, M. and Verges, M. (2012). Retromer regulates postendocytic sorting of β-secretase in polarized Madin-Darby canine kidney cells. *Traffic* **13**, 1393-1410. doi:10.1111/j.1600-0854.2012.01392.x

Delacour, D., Koch, A. and Jacob, R. (2009). The role of galectins in protein trafficking. *Traffic* **10**, 1405-1413. doi:10.1111/j.1600-0854.2009.00960.x

Dessau, R. B. and Pipper, C. B. (2008). ["'R"–project for statistical computing]. *Ugeskr. Laeger.* **170**, 328-330.

Drisdel, R. C. and Green, W. N. (2004). Labeling and quantifying sites of protein palmitoylation. *BioTechniques* **36**, 276-285. doi:10.2144/04362RR02

Dulsat, G., Palomeras, S., Cortada, E., Riuró, H., Brugada, R. and Vergés, M. (2017). Trafficking and localisation to the plasma membrane of $Na_v1.5$ promoted by the β2 subunit is defective due to a β2 mutation associated with Brugada syndrome. *Biol. Cell* **109**, 273-291. doi:10.1111/boc.201600085

Fenton, R. G., Kung, H. F., Longo, D. L. and Smith, M. R. (1992). Regulation of intracellular actin polymerization by prenylated cellular proteins. *J. Cell Biol.* **117**, 347-356. doi:10.1083/jcb.117.2.347

Füllekrug, J., Shevchenko, A., Shevchenko, A. and Simons, K. (2006). Identification of glycosylated marker proteins of epithelial polarity in MDCK cells by homology driven proteomics. *BMC Biochem.* **7**, 8. doi:10.1186/1471-2091-7-8

Gillet, L., Shy, D. and Abriel, H. (2014). Elucidating sodium channel Nav1.5 clustering in cardiac myocytes using super-resolution techniques. *Cardiovasc. Res.* **104**, 231-233. doi:10.1093/cvr/cvu221

Gottlieb, T. A., Ivanov, I. E., Adesnik, M. and Sabatini, D. D. (1993). Actin microfilaments play a critical role in endocytosis at the apical but not the basolateral surface of polarized epithelial cells. *J. Cell Biol.* **120**, 695-710. doi:10.1083/jcb.120.3.695

Haft, C. R., de la Luz Sierra, M., Bafford, R., Lesniak, M. A., Barr, V. A. and Taylor, S. I. (2000). Human orthologs of yeast vacuolar protein sorting proteins Vps26, 29, and 35: assembly into multimeric complexes. *Mol. Biol. Cell* **11**, 4105-4116. doi:10.1091/mbc.11.12.4105

Head, B. P., Patel, H. H. and Insel, P. A. (2014). Interaction of membrane/lipid rafts with the cytoskeleton: impact on signaling and function: membrane/lipid rafts, mediators of cytoskeletal arrangement and cell signaling. *Biochim. Biophys. Acta (BBA) Biomembr.* **1838**, 532-545. doi:10.1016/j.bbamem.2013.07.018

Janich, P. and Corbeil, D. (2007). GM_1 and GM_3 gangliosides highlight distinct lipid microdomains within the apical domain of epithelial cells. *FEBS Lett.* **581**, 1783-1787. doi:10.1016/j.febslet.2007.03.065

Johnson, D. and Bennett, E. S. (2006). Isoform-specific effects of the β2 subunit on voltage-gated sodium channel gating. *J. Biol. Chem.* **281**, 25875-25881. doi:10.1074/jbc.M605060200

Kang, M., Day, C. A., Kenworthy, A. K. and DiBenedetto, E. (2012). Simplified equation to extract diffusion coefficients from confocal FRAP data. *Traffic* **13**, 1589-1600. doi:10.1111/tra.12008

Keller, P. and Simons, K. (1998). Cholesterol is required for surface transport of influenza virus hemagglutinin. *J. Cell Biol.* **140**, 1357-1367. doi:10.1083/jcb.140.6.1357

Kusumi, A., Fujiwara, T. K., Tsunoyama, T. A., Kasai, R. S., Liu, A.-A., Hirosawa, K. M., Kinoshita, M., Matsumori, N., Komura, N., Ando, H. et al. (2020). Defining raft domains in the plasma membrane. *Traffic* **21**, 106-137. doi:10.1111/tra.12718

Kyle, J. W. and Makielski, J. C. (2014). Diseases caused by mutations in Nav1.5 interacting proteins. *Card. Electrophysiol. Clin.* **6**, 797-809. doi:10.1016/j.ccep.2014.08.007
Le Bivic, A., Garcia, M. and Rodriguez-Boulan, E. (1993). Ricin-resistant Madin-Darby canine kidney cells missort a major endogenous apical sialoglycoprotein. *J. Biol. Chem.* **268**, 6909-6916. doi:10.1016/S0021-9258(18)53126-4
Levental, I., Levental, K. R. and Heberle, F. A. (2020). Lipid Rafts: controversies resolved, mysteries remain. *Trends Cell Biol.* **30**, 341-353. doi:10.1016/j.tcb.2020.01.009
Marlar, S., Arnspang, E. C., Pedersen, G. A., Koffman, J. S. and Nejsum, L. N. (2014). Measuring localization and diffusion coefficients of basolateral proteins in lateral versus basal membranes using functionalized substrates and kICS analysis. *Biochim. Biophys. Acta (BBA) Biomembr.* **1838**, 2404-2411. doi:10.1016/j.bbamem.2014.06.005
Mellado, M., Cuartero, Y., Brugada, R. and Verges, M. (2014). Subcellular localisation of retromer in post-endocytic pathways of polarised Madin–Darby canine kidney cells. *Biol. Cell* **106**, 377-393. doi:10.1111/boc.201400011
Napolitano, C. and Priori, S. G. (2006). Brugada syndrome. *Orphanet J. Rare Dis.* **1**, 35. doi:10.1186/1750-1172-1-35
O'Malley, H. A. and Isom, L. L. (2015). Sodium channel β subunits: emerging targets in channelopathies. *Annu. Rev. Physiol.* **77**, 481-504. doi:10.1146/annurev-physiol-021014-071846
Peran, M., Hicks, B. W., Peterson, N. L., Hooper, H. and Salas, R. (2001). Lateral mobility and anchoring of recombinant GABAA receptors depend on subunit composition. *Cell Motil. Cytoskeleton* **50**, 89-100. doi:10.1002/cm.1043
Phair, R. D. and Misteli, T. (2001). Kinetic modelling approaches to in vivo imaging. *Nat. Rev. Mol. Cell Biol.* **2**, 898-907. doi:10.1038/35103000
Pralle, A., Keller, P., Florin, E.-L., Simons, K. and Hörber, J. K. H. (2000). Sphingolipid-cholesterol rafts diffuse as small entities in the plasma membrane of mammalian cells. *J. Cell Biol.* **148**, 997-1008. doi:10.1083/jcb.148.5.997
Reverter, M., Rentero, C., de Muga, S. V., Alvarez-Guaita, A., Mulay, V., Cairns, R., Wood, P., Monastyrskaya, K., Pol, A., Tebar, F. et al. (2011). Cholesterol transport from late endosomes to the Golgi regulates t-SNARE trafficking, assembly, and function. *Mol. Biol. Cell* **22**, 4108-4123. doi:10.1091/mbc.e11-04-0332r
Riuró, H., Beltran-Alvarez, P., Tarradas, A., Selga, E., Campuzano, O., Vergés, M., Pagans, S., Iglesias, A., Brugada, J., Brugada, P. et al. (2013). A missense mutation in the sodium channel β2 subunit reveals SCN2B as a new candidate gene for Brugada syndrome. *Hum. Mutat.* **34**, 961-966. doi:10.1002/humu.22328
Rivaud, M. R., Delmar, M. and Remme, C. A. (2020). Heritable arrhythmia syndromes associated with abnormal cardiac sodium channel function: ionic and non-ionic mechanisms. *Cardiovasc. Res.* **116**, 1557-1570. doi:10.1093/cvr/cvaa082
Rodriguez-Boulan, E. and Macara, I. G. (2014). Organization and execution of the epithelial polarity programme. *Nat. Rev. Mol. Cell Biol.* **15**, 225-242. doi:10.1038/nrm3775
Rook, M. B., Evers, M. M., Vos, M. A. and Bierhuizen, M. F. A. (2012). Biology of cardiac sodium channel Nav1.5 expression. *Cardiovasc. Res.* **93**, 12-23. doi:10.1093/cvr/cvr252
Salvage, S. C., Huang, C. L.-H. and Jackson, A. P. (2020). Cell-adhesion properties of β-subunits in the regulation of cardiomyocyte sodium channels. *Biomolecules* **10**, 989. doi:10.3390/biom10070989
Schmidt, J. W. and Catterall, W. A. (1986). Biosynthesis and processing of the α subunit of the voltage-sensitive sodium channel in rat brain neurons. *Cell* **46**, 437-445. doi:10.1016/0092-8674(86)90664-1
Sharpe, H. J., Stevens, T. J. and Munro, S. (2010). A comprehensive comparison of transmembrane domains reveals organelle-specific properties. *Cell* **142**, 158-169. doi:10.1016/j.cell.2010.05.037
Shipston, M. J. (2014). Ion channel regulation by protein S-acylation. *J. Gen. Physiol.* **143**, 659-678. doi:10.1085/jgp.201411176
Shvartsman, D. E., Gutman, O., Tietz, A. and Henis, Y. I. (2006). Cyclodextrins but not compactin inhibit the lateral diffusion of membrane proteins independent of cholesterol. *Traffic* **7**, 917-926. doi:10.1111/j.1600-0854.2006.00437.x
Simons, K. and Sampaio, J. L. (2011). Membrane organization and lipid rafts. *Cold Spring Harb. Perspect. Biol.* **3**, a004697. doi:10.1101/cshperspect.a004697
Sprague, B. L. and McNally, J. G. (2005). FRAP analysis of binding: proper and fitting. *Trends Cell Biol.* **15**, 84-91. doi:10.1016/j.tcb.2004.12.001
Stevenson, B. R., Siliciano, J. D., Mooseker, M. S. and Goodenough, D. A. (1986). Identification of ZO-1: a high molecular weight polypeptide associated with the tight junction (zonula occludens) in a variety of epithelia. *J. Cell Biol.* **103**, 755-766. doi:10.1083/jcb.103.3.755
Stoops, E. H. and Caplan, M. J. (2014). Trafficking to the apical and basolateral membranes in polarized epithelial cells. *J. Am. Soc. Nephrol.* **25**, 1375-1386. doi:10.1681/ASN.2013080883
UniProt Consortium. (2019). UniProt: a worldwide hub of protein knowledge. *Nucleic Acids Res.* **47**, D506-D515. doi:10.1093/nar/gky1049
Valdivia, C. R., Medeiros-Domingo, A., Ye, B., Shen, W.-K., Algiers, T. J., Ackerman, M. J. and Makielski, J. C. (2010). Loss-of-function mutation of the SCN3B-encoded sodium channel β3 subunit associated with a case of idiopathic ventricular fibrillation. *Cardiovasc. Res.* **86**, 392-400. doi:10.1093/cvr/cvp417
Vergés, M., Sebastián, I. and Mostov, K. E. (2007). Phosphoinositide 3-kinase regulates the role of retromer in transcytosis of the polymeric immunoglobulin receptor. *Exp. Cell Res.* **313**, 707-718. doi:10.1016/j.yexcr.2006.11.010
Verkade, P., Harder, T., Lafont, F. and Simons, K. (2000). Induction of caveolae in the apical plasma membrane of Madin-Darby canine kidney cells. *J. Cell Biol.* **148**, 727-740. doi:10.1083/jcb.148.4.727
Wan, J., Roth, A. F., Bailey, A. O. and Davis, N. G. (2007). Palmitoylated proteins: purification and identification. *Nat. Protoc.* **2**, 1573-1584. doi:10.1038/nprot.2007.225
Weisz, O. A. and Rodriguez-Boulan, E. (2009). Apical trafficking in epithelial cells: signals, clusters and motors. *J. Cell Sci.* **122**, 4253-4266. doi:10.1242/jcs.032615
Wong, H.-K., Sakurai, T., Oyama, F., Kaneko, K., Wada, K., Miyazaki, H., Kurosawa, M., De Strooper, B., Saftig, P. and Nukina, N. (2005). β subunits of voltage-gated sodium channels are novel substrates of β-site amyloid precursor protein-cleaving enzyme (BACE1) and γ-secretase. *J. Biol. Chem.* **280**, 23009-23017. doi:10.1074/jbc.M414648200
Zidovetzki, R. and Levitan, I. (2007). Use of cyclodextrins to manipulate plasma membrane cholesterol content: evidence, misconceptions and control strategies. *Biochim. Biophys. Acta (BBA) Biomembr.* **1768**, 1311-1324. doi:10.1016/j.bbamem.2007.03.026
Zimmer, T., Biskup, C., Bollensdorff, C. and Benndorf, K. (2002). The beta1 subunit but not the beta2 subunit colocalizes with the human heart Na+ channel (hH1) already within the endoplasmic reticulum. *J. Membr. Biol.* **186**, 13-21. doi:10.1007/s00232-001-0131-0
Zurzolo, C. and Simons, K. (2016). Glycosylphosphatidylinositol-anchored proteins: membrane organization and transport. *Biochim. Biophys. Acta (BBA) Biomembr.* **1858**, 632-639. doi:10.1016/j.bbamem.2015.12.018